Applied Ocean Research 126 (2022) 103280

Contents lists available at ScienceDirect

Applied Ocean Research

journal homepage: www.elsevier.com/locate/apor

Hydrodynamic performance of a new-type vertical wall breakwater with inclined culvert on a permeable rubble mound foundation

Chaofan Lv [a], Xizeng Zhao [b,c,*], Mingchang Li [c]

[a] College of Civil Engineering and Architecture, Zhejiang University, Hangzhou 310058, Zhejiang, China
[b] Ocean College, Zhejiang University, Zhoushan 316021, Zhoushan, China
[c] School of Marine Engineering Equipment, Zhejiang Ocean University, Zhoushan, 316022, Zhejiang, China

ARTICLE INFO

Keywords:
Vertical wall breakwater with inclined culvert
Permeable rubble mound foundation
Eigenfunction expansion boundary element method
Hydrodynamic performance
Energy dissipation

ABSTRACT

Vertical wall breakwater with inclined culvert (VWBIC) is a new-type environmentally friendly breakwater proposed in this paper, which is a further development of vertical wall breakwater with horizontal culvert (Lv and Zhao, 2021). To analyze the hydrodynamic performance of the VWBIC on a permeable rubble mound foundation and to propose the optimal structural parameters of the culvert for engineering application, an eigenfunction expansion boundary element method (EEBEM) is used. Besides, newly performed computational fluid dynamics (CFD) results are used to reveal the interaction mechanism between waves and the VWBIC. The results show that when the culvert inclined angle is positive, the VWBIC is more beneficial to engineering application. With an increase in the culvert inclined angle, the VWBIC can effectively reduce wave transmission coefficient of medium and long waves, promote the oscillatory flow of short waves and reduce the wave force on the VWBIC. Meanwhile, through the effects of wave shallowing, resonance and energy dissipation, the permeable rubble mound foundation can significantly reduce the wave reflection and wave force on the VWBIC. Finally, the optimal structural parameters of the VWBIC are obtained. All these indicate that the VWBIC is a more effective structure than vertical wall breakwater with horizontal culvert.

1. Introduction

Breakwater with culvert (BC) is a kind of environmentally friendly breakwater for coastal and offshore engineering (Tsoukala and Moutzouris, 2009; Rageh and Koraim, 2010). Compared with the gravity breakwater, the BC can effectively reduce wave reflection and wave force on the breakwater (Li et al., 1997b), promote water exchange, and reduce the sediment deposition in the harbor basin (Lv and Zhao, 2021). Besides, some aquatic organisms can freely pass through the culvert, which is of great significance to maintaining the aquatic ecological environment in the harbor basin (Tsoukala et al., 2014). However, the distribution of sediment concentration in the ocean follows the law of being sparse at the top and dense at the bottom, especially for the encircled harbor basin. To further promote the water exchange and reduce sediment deposition, a new-type vertical wall breakwater with inclined culvert (VWBIC) is proposed in this paper, and it is a further study of vertical wall breakwater with horizontal culvert (Lv and Zhao, 2021). When the culvert inlet (sea area) is higher than the culvert outlet (harbor area), the high turbidity water at the bottom of the harbor will flow into the sea through oscillatory flow, and the low turbidity water at the surface of sea will flush the harbor area. It could be expected that due to this special setting, VWBIC will have a good effect on water exchange.

In practice, the location of the culvert can be set at sea level or under water for different tide types. When the BC is placed in a weak tidal range area, the culvert placed at sea level is better than that placed under water. This breakwater is called breakwater with flushing culvert. Due to the sudden changes of the topography, waves in the culvert will be broken, and the oscillatory flow in the culvert can also play a good role in flushing the harbor basin (Tsoukala and Moutzouris, 2009; Belibassakis et al., 2014). When the BC is placed in the large tidal range areas, the culvert placed under water is superior due to the significant change of sea level (Li et al., 1997a; Lv and Zhao, 2021). It can effectively promote water exchange between the harbor basin and offshore area due to the action of tides and waves. From the above, it can be found that different tide types have a great impact on the culvert. However, if the culvert is arranged at an inclined angle, it will not be affected by the tides and has stronger applicability. On the one hand, the culvert inlet located near the sea level can facilitate wave breaking. On the other hand, because the culvert is inclined, the proper layout can also keep the culvert below the sea level for water exchange.

* Corresponding author at: Ocean College, Zhejiang University, Zhoushan 316021, Zhoushan, China.
E-mail addresses: chaofanlvgg@gmail.com (C. Lv), xizengzhao@zju.edu.cn (X. Zhao).

https://doi.org/10.1016/j.apor.2022.103280
Received 25 March 2022; Received in revised form 4 June 2022; Accepted 8 July 2022
Available online 18 July 2022

Over the years, many researchers have been dedicated to studying the interaction between waves and the BC (Zhu and Chwang, 2001; Suh et al., 2006, 2007). Li et al. (1997a,b) analyzed the wave force on the vertical wall breakwater with culvert (VWBC) and reflection coefficient based on potential flow theory, and they found that the VWBC can effectively reduce the wave force and wave reflection coefficient. Subsequently, some experiments and numerical simulations mainly focused on the geometric characteristics of culverts and the influence of incident wave height on the wave deformation (Tsoukala and Moutzouris, 2008, 2009), harmonic wave (Tsoukala et al., 2010, 2014) and the oscillatory flow in the culvert (Carevic et al., 2018; Bartolić et al., 2018). They found that the size of the culvert and the incident wave have a great influence on the water exchange, while the generation and transmission coefficient of harmonics are mainly affected by the width of the culvert. Although they found that the culvert has great effects on the hydrodynamic performance of the BC, there was no relevant design theory to explain how to choose the optimal culvert. Lv and Zhao (2021) adopted theoretical, numerical and experimental methods to study the hydrodynamic characteristics of VBWC, and proposed a calculation method to calculate the optimal culvert. The results show that the culvert height and culvert depth are the main factors which affect the hydrodynamic performance of the VWBC.

In reality, breakwaters are usually built on a permeable rubble mound foundation, and the permeable rubble mound foundation has great effects on the hydrodynamic performance of the breakwater. Up to now, a great deal of research has been carried out on the interaction between wave and permeable structure (Madsen, 1974; Liu et al., 1999; Del Jesus et al., 2012). Dalrymple et al. (1991) estimated wave reflection and transmission of rectangular uniform porous structure under oblique incident wave action by eigenfunction expansion method. Requejo et al. (2002) derived the reflection and transmission coefficient of vertical permeable breakwater, and analyzed the effects of dimensionless parameters such as structure width, stone size, porosity on the stability of porous breakwaters. Subsequently, a series of studies were carried out by using the (Sollitt and Cross, 1973) models of wave passing through the porous structures, such as porous structures near a wall (Koley et al., 2015a), underwater trapezoidal porous breakwater (Koley et al., 2015b), submerged semicircular porous breakwater (Koley and Sahoo, 2017), rubble mound offshore porous breakwaters (Koley et al., 2020). It is found that reasonable arrangement of permeable breakwater can effectively promote the dissipation of wave energy and reduce wave reflection and wave force. Similarly, the research of Zhao et al. (2016) further confirmed the role of porous structure.

The aforementioned studies have well analyzed the hydrodynamic performance of the BC and the permeable rubble mound foundation, and provided valuable results for practice. However, since the VWBIC is first put forward in this paper, there has been no research on its hydrodynamic performance. Besides, the influence of permeable rubble mound foundation on the VWBIC has not been discussed till now. The optimal structural parameters of the inclined culvert will change, so it is still necessary and important to find the optimal solution. Therefore, in this paper, a coupled eigenfunction expansion boundary element method (EEBEM) (Koley et al., 2020; Rodríguez et al., 2022) and computational fluid dynamics (CFD) numerical simulation (Zhao et al., 2014) are used to comprehensively study the hydrodynamic performance of the VWBIC, and then the optimal structural parameters of the culvert are proposed to provide a reference for engineering application.

The EEBEM is a method which couples eigenfunction expansion method (Deng et al., 2019) with multi-domain boundary element method (Chen et al., 2017; Zhao et al., 2020). Unlike theoretical analysis (Liu and Li, 2013; Koley et al., 2015a; Li et al., 2020), the EEBEM has no restriction on the shape of structures. Therefore, it can solve many complicated problems, such as the interaction between the waves and the VWBIC. Meanwhile, compared with the multi-domain boundary element method (Bakhti et al., 2017), it can be more accurately to solve the problem of wave interaction with structures, and it can effectively reduce the computational domain and improve the calculation speed. Besides, the results obtained by the EEBEM are basically consistent with the analytical results. Through the EEBEM, the velocity potential of any point in the computational domain can be obtained. Then the corresponding wave force, wave transmission coefficient and oscillatory flow can be derived.

In the next section, the implementation of the EEBEM is described in detail. Then, the CFD model of the VWBIC is briefly introduced in Section 3, and the interaction between waves and the VWBIC is revealed by CFD results. In Section 4, the hydrodynamic performances of the VWBIC are demonstrated through the EEBEM, and the effects of the culvert inclined angle and permeable rubble mound foundation are analyzed emphatically. In addition, the EEBEM is also used to obtain the optimal structural parameters of the culvert. Finally, the main conclusions are given.

2. Model of coupled eigenfunction expansion boundary element method (EEBEM)

2.1. Governing equations and boundary conditions

The sketch of a vertical wall breakwater with inclined culvert (VWBIC) is shown in Fig. 1, in which the x-axis is the still water surface and the z-axis is pointing upwards. Assuming that A_i is the incident wave amplitude; H_i is the incident wave height; T_i is the incident wave period; h_1 is the far field water depth; h_2 is the water depth on the permeable rubble mound foundation; L_p is the length of the permeable rubble mound foundation; d_1 and d_2 are the draft of the upper structure; d_3 and d_4 are the distance from the bottom of culvert to the still water surface; ΔS is the culvert inlet height and $\Delta S = (d_2 - d_1) = (d_4 - d_3)$; d_n is the distance of culvert middle longitudinal axis apart from the still water surface; S is the culvert height; θ is the culvert inclined angle and $S = \Delta S * \cos(\theta)$; the length of the VWBIC is $2B$; H_r and H_t are the height of reflection waves and transmission waves, respectively. In addition, Γ_l setting at $x = -l$ is the wave inlet boundary and Γ_r setting at $x = r$ is the wave outlet boundary. Γ_{F1} and Γ_{F2} are the wave surface boundary; Γ_{F3} is the upper structure boundary of the VWBIC. Γ_{B1} and Γ_{B2} are the water bottom boundary, and Γ_{B3} is the breakwater lower structure boundary. Γ_{P1} is the interface between the rubble mound foundation and the fluid domain; Γ_{P2} is the interface between the rubble mound foundation and the VWBIC; and Γ_{P3} is the interface between the rubble mound foundation and water bottom.

Considering that the problem satisfying linear wave theory and the velocity potential can be expressed as $\Phi(x,z,t) = \mathrm{Re}[\phi(x,z)e^{-i\sigma t}]$ (where Re[ ] denotes the real parts of a complex, σ is the circular frequency, $i = \sqrt{-1}$, $\phi(x,z)$ is the complex amplitude of the velocity potential). Then the total fluid domain is divided into four sub-regions ($\Omega_1, \Omega_2, \Omega_3, \Omega_4$) and the velocity potential in each sub-regions is assumed as $\phi_1, \phi_2, \phi_3, \phi_4$, where Ω_1 and Ω_3 are the outer region for wave inlet and outlet; Ω_2 is the inner region outside the VWBIC and the permeable rubble mound foundation, and Ω_4 is the inner region for the permeable rubble mound foundation. Under the linear wave theory, velocity potential ϕ should satisfy the following governing equation and boundary conditions:

$$\nabla^2 \phi_s(x,z) = 0, \quad \text{for } s = 1,2,3,4. \tag{1}$$

The linearized free surface boundary condition is given by:

$$\frac{\partial \phi_s}{\partial \boldsymbol{n}} = K\phi_s, \quad \text{for } s = 1,2,3, \text{ on } z = 0, \tag{2}$$

where $K = \sigma^2/g$, g is the gravitational acceleration, $\boldsymbol{n}$ is the normal direction and the impermeable bottom boundary condition can be

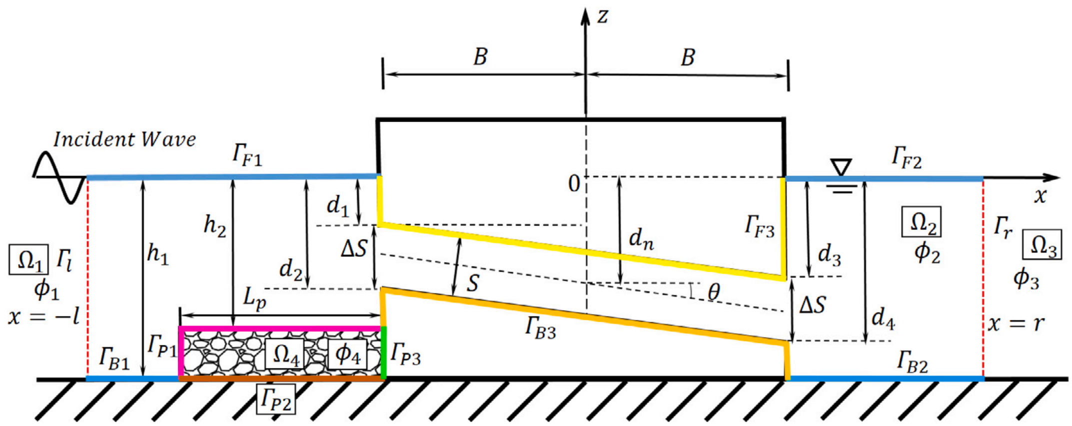

Fig. 1. Schematic diagram of vertical wall breakwater with inclined culvert.

expressed as:

$$\frac{\partial \phi_s}{\partial \boldsymbol{n}} = 0, \quad \text{for } s = 2 \text{ on } \Gamma_{F3}, \Gamma_{B1}, \Gamma_{B2}, \Gamma_{B3},\ s = 4 \text{ on } \Gamma_{P2}, \Gamma_{P3}, \text{ and } \quad s = 1, 3 \text{ on } z = -h_1, \tag{3}$$

At the interfaces between the sub-regions Ω_2 and Ω_4, the continuity of pressure and mass flux yield should satisfy

$$\begin{cases} \phi_2 = (m_p + i f_p)\phi_4 \\ \frac{\partial \phi_2}{\partial \boldsymbol{n}} = -\varepsilon \frac{\partial \phi_4}{\partial \boldsymbol{n}} \end{cases}, \quad \text{on } \Gamma_{P1}, \tag{4}$$

where m_p and f_p are the inertial and friction coefficients respectively and ε is the porosity of the rubble mound foundation.

The radiation conditions in the far fields can be expressed as:

$$\begin{cases} \frac{\partial(\phi_1 - \phi_0)}{\partial x} + i k_0(\phi_1 - \phi_0) = 0, & \text{as } x \to -\infty \\ \frac{\partial \phi_3}{\partial x} - i k_0 \phi_3 = 0, & \text{as } x \to +\infty \end{cases}, \tag{5}$$

where $\phi_0 = e^{ik_0(x+l)} f_0(k_0, z)$ is the incident wave; k_0 is the wavenumber, and $f_0(k_0, z)$ is expressed as Eq. (10).

The continuity of pressure and velocity on Γ_l and Γ_r are written as:

$$\phi_2 = \begin{cases} \phi_1, & \text{on } \Gamma_l \\ \phi_3, & \text{on } \Gamma_r \end{cases}, \quad \frac{\partial \phi_2}{\partial \boldsymbol{n}} = \begin{cases} -\frac{\partial \phi_1}{\partial n} = -\frac{\partial \phi_1}{\partial x}, & \text{on } \Gamma_l \\ -\frac{\partial \phi_3}{\partial n} = \frac{\partial \phi_3}{\partial x}, & \text{on } \Gamma_r \end{cases}, \tag{6}$$

2.2. Solution of coupled eigenfunction expansion boundary element method (EEBEM)

The eigenfunction expansion boundary element method (EEBEM) is a suitable way to solve the interaction between waves and the VWBIC, in which the eigenfunction expansion method is used to obtain the complex potential ϕ_1 and ϕ_3 in the outer region, and the multi-domain boundary element method is used to transform the boundary value problems in the inner region into the integral equations. To reduce the calculation time, Γ_l and Γ_r are situated $h_1/2$ away from the VWBIC, and the influence of evanescent wave modes is considered to improve the accuracy of the model.

The complex potential ϕ_1 and ϕ_3 in the outer region can be written as:

$$\phi_1 = e^{ik_0(x+l)} f_0(k_0, z) + \sum_{m=0}^{\infty} R_m e^{-ik_m(x+l)} f_m(k_m, z), \tag{7}$$

$$\phi_3 = \sum_{m=0}^{\infty} T_m e^{ik_m(x-r)} f_m(k_m, z), \tag{8}$$

where R_m and T_m $(m = 0, 1, 2, \dots)$ are the undetermined coefficient, m is the velocity potential expansion terms, k_m $(m = 0, 1, 2, \dots)$ satisfies Eq. (9)

$$\sigma^2 = g k_m \tanh k_m h_1, \qquad m = 0, 1, 2 \dots, \tag{9}$$

where k_0 is real number and k_m $(m = 1, 2, \dots)$ is imaginary number. It may be noted that k_m $(m = 1, 2, \dots)$ is in the form of $k_m = k'_m i$, where k'_m is the real positive roots of $\sigma^2 = -g k'_m \tan k'_m h_1$.

The eigenfunction $f(k_0, z)$ and $f(k_m, z)$ satisfy the following equation:

$$f_m(k_m, z) = -\frac{igA_i}{\sigma} \frac{\cosh k_m(z + h_1)}{\cosh k_m h_1} \qquad m = 0, 1, 2 \dots M, \tag{10}$$

Besides, $\langle .,. \rangle$ is denoted the inner product. According to orthogonality, the inner product of $f(k_m, z)$ and $f(k_n, z)$ can be expressed as:

$$\langle f(k_m, z), f(k_n, z) \rangle = \int_{-h}^{0} f(k_m, z) f(k_n, z) dz = S_n \delta_{mn}, \tag{11}$$

where $S_n = -\left(\frac{gA_i}{\sigma}\right)^2 \left[\frac{\sinh(2k_n h_1) + 2k_n h_1}{4(k_n)\cosh^2(k_n h_1)}\right]$, and δ is Kronecker function.

According to Eqs. (7) and (11), the unknown coefficient R_m can be expressed as:

$$R_m + \delta_{m0} = \frac{1}{S_m} \left\langle \widehat{\phi_2}, f_m(k_m, z) \right\rangle, \tag{12}$$

where $\widehat{\phi_2}$ represents the velocity potential when the expansion term $m = M$.

According to Eq. (7), the normal derivative of ϕ_1 can be written as:

$$\frac{\partial \phi_1}{\partial \boldsymbol{n}} = i k_0 e^{ik_0(x+l)} f_0(k_0, z) - \sum_{m=0}^{\infty} R_m i k_m e^{-ik_m(x+l)} f_m(k_m, z). \tag{13}$$

Substitute Eqs. (12) and (13) into Eq. (6), the boundary condition on Γ_l can be written as:

$$\left.\frac{\partial \phi_2}{\partial \boldsymbol{n}}\right|_{x=-l} = \sum_{m=0}^{M} \frac{i k_m f_m(k_m, z)}{S_m} \left\langle \widehat{\phi_2}, f_m(k_m, z) \right\rangle - 2 i k_0 f_0(k_0, z), \quad \text{on } \Gamma_l, \tag{14}$$

Similarly, the boundary condition on Γ_r can be expressed as:

$$T_m = \frac{1}{S_m} \left\langle \widehat{\phi_2}, f_m(k_m, z) \right\rangle, \tag{15}$$

$$\left.\frac{\partial \phi_2}{\partial \boldsymbol{n}}\right|_{x=r} = \sum_{m=0}^{M} \frac{i k_m f_m(k_m, z)}{S_m} \left\langle \widehat{\phi_2}, f_m(k_m, z) \right\rangle, \quad \text{on } \Gamma_r, \tag{16}$$

As can be seen from the above, all the boundary conditions of inner region Ω_2 and Ω_4 are the functions of ϕ and $\frac{\partial \phi}{\partial n}$. To calculate ϕ and $\frac{\partial \phi}{\partial n}$ in inner region Ω_2 and Ω_4, the boundary of inner region Ω_2 and Ω_4 are divided into J_1 and J_2 finite elements respectively, and the element length dl of each element is equal. For more details of computation length and mesh discretization, refer to Section 2.4.1. Then, according to the above boundary conditions, $(J_1 + J_2)$ equation system can be established. Besides, for inner region Ω_2 and Ω_4, $(J_1 +$

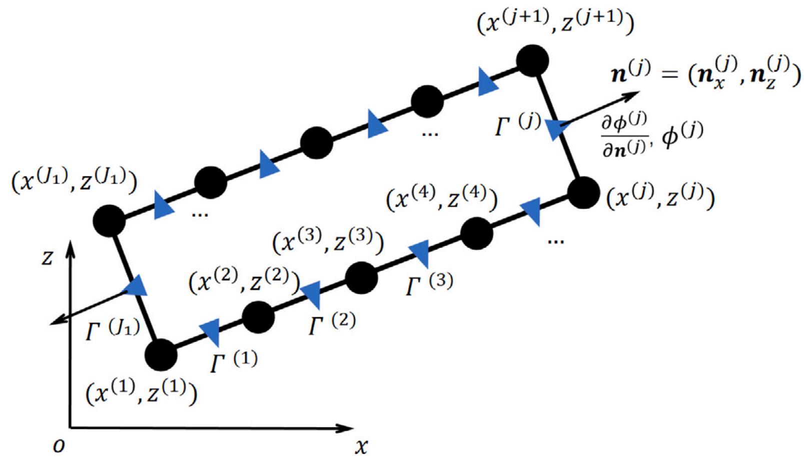

Fig. 2. Schematic diagram of solution domain of boundary element method.

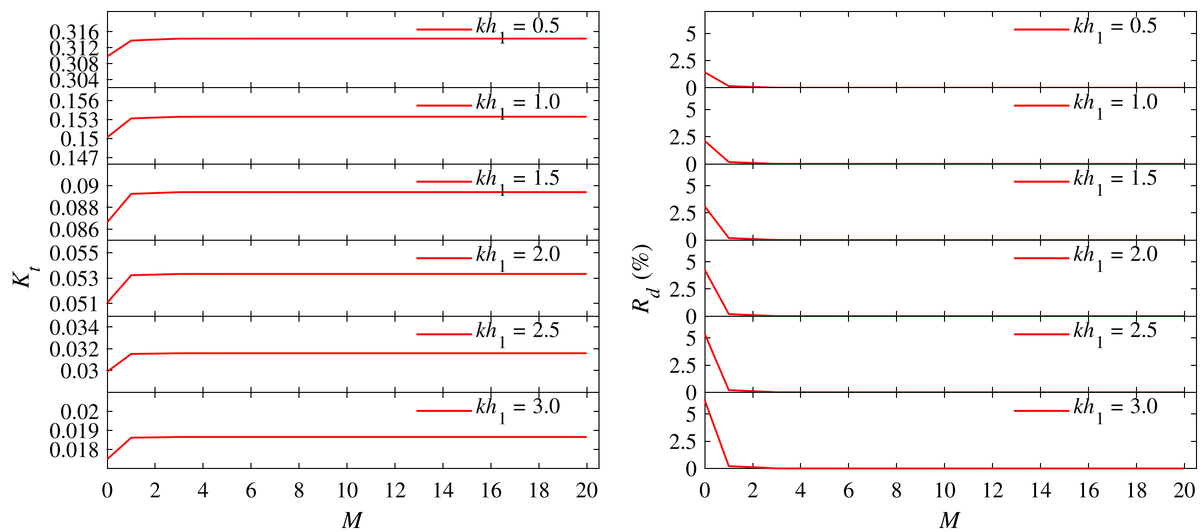

(a) Wave transmission coefficient K_t (b) Relative difference R_d of K_t

Fig. 3. Convergence tests of K_t and R_d with different truncated numbers M. $h_1 = 0.4$ m, $h_2 = 0.36$ m, $B = 0.2$ m, $S = 0.04$ m, $d_n = 0.2$ m, $\theta = 20°$, $L_p = 0.16$ m, $\varepsilon = 0.8, m_p = 1, f_p = 0.2$, $dl = 0.002$ m.

J_2) boundary integral equations can be established by Green's second theorem. Finally, the value of ϕ and $\frac{\partial \phi}{\partial n}$ at the boundary can be obtained through the $2(J_1 + J_2)$ equation system.

The boundary integral equation of Ω_2 and Ω_4 are expressed as:

$$\lambda(\xi,\eta)\phi(\xi,\eta) = \int_\Gamma \left[\phi(x,z)\frac{\partial G(x,z;\xi,\eta)}{\partial \boldsymbol{n}} - G(x,z;\xi,\eta)\frac{\partial \phi(x,z)}{\partial \boldsymbol{n}}\right] d\Gamma(x,z), \tag{17}$$

$$\lambda(\xi,\eta) = \begin{cases} 0.5, & \text{if } (\xi,\eta) \text{ on the } \Gamma \\ 1, & \text{if } (\xi,\eta) \in \Omega, \text{ but not on the } \Gamma \end{cases}. \tag{18}$$

where (ε, η) is the source point; Γ represents the boundary of Ω_2 or Ω_4; $G(x,z;\xi,\eta)$ is the Green's function and it is written as:

$$G(x,z;\xi,\eta) = \frac{\ln(r)}{2\pi}, \quad r = \sqrt{(x-\xi)^2 + (z-\eta)^2}, \quad \text{for } (x,z) \neq (\xi,\eta), \tag{19}$$

Fig. 2 shows schematic diagram of solution domain (Ω_2 or Ω_4) of boundary element method. The boundary of inner region Ω_2 and Ω_4 are divided into J_1 and J_2 finite boundary elements, respectively. For an arbitrary boundary element $\Gamma^{(j)}$, $(x^{(j)}, z^{(j)})$ is the starting point; $(x^{(j+1)}, z^{(j+1)})$ is the ending point; $\boldsymbol{n}^{(j)} = (n_x^{(j)}, n_z^{(j)})$ is the normal vector of the element; $\phi^{(j)}$ and $\frac{\partial \phi^{(j)}}{\partial n}$ are the velocity potential and normal derivative of the velocity potential. Based on Eq. (17), the original continuous solution is expressed as:

$$\lambda(\xi,\eta)\phi(\xi,\eta) = \sum_{j=1}^{J_1} \left\{ \overline{\phi}^{(j)} F_2{}^{(j)}(\xi,\eta) - \overline{p}^{(j)} F_1{}^{(j)}(\xi,\eta) \right\}, \quad \text{for the boundary of } \Omega_2, \tag{20}$$

$$\lambda(\xi,\eta)\phi(\xi,\eta) = \sum_{j=1}^{J_2} \left\{ \overline{\phi}^{(j)} F_2{}^{(j)}(\xi,\eta) - \overline{p}^{(j)} F_1{}^{(j)}(\xi,\eta) \right\}, \quad \text{for the boundary of } \Omega_4, \tag{21}$$

where

$$\phi \simeq \overline{\phi}^{(j)}, \text{ and } \frac{\partial \phi}{\partial \boldsymbol{n}} = \overline{p}^{(j)} \text{ for } (x,z) \in \Gamma^{(j)} \ (j = 1,2,\ldots J_1 \text{ or } J_2), \tag{22}$$

$$\begin{aligned} F_1{}^{(j)}(\xi,\eta) &= \int_{\Gamma^{(j)}} G(x,z;\xi,\eta) d\Gamma(x,z), \\ F_2{}^{(j)}(\xi,\eta) &= \int_{\Gamma^{(j)}} \frac{\partial}{\partial n} G(x,z;\xi,\eta) d\Gamma(x,z), \end{aligned} \tag{23}$$

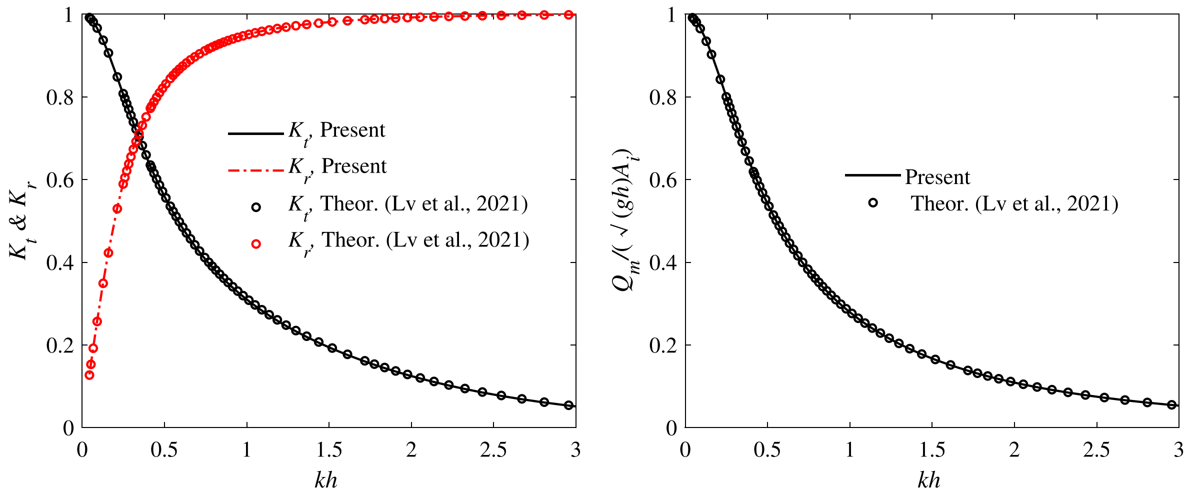

(a) Wave transmission coefficient K_t and reflection coefficient K_r

(b) Maximum oscillatory flow Q_m

Fig. 4. Comparisons of K_r, K_t and Q_m between the present EEBEM results and theoretical solutions of Lv and Zhao (2021). $h_1 = h_2 = h = 0.4$ m, $B = 0.25$ m, $d_n = 0.177$ m, $S = 0.096$ m, $\theta = 0$, $L_p = 0$ m.

where $\overline{\phi}^{(j)}$ and $\overline{p}^{(j)}$ are the values of the element $\Gamma^{(j)}$, and the midpoint is used to represent it.

Actually, the boundary integral Eqs. (20) and (21) are independent, and they are coupled together by Eq. (4). Then, through Eq. (2), (3), (4), (14), (16), (20) and (21), ϕ and $\frac{\partial \phi}{\partial n}$ at the boundary of Ω_2 and Ω_4 can be obtained. The wave transmission coefficient K_t and reflection coefficient K_r can be written as:

$$K_r = |R_0| = \left| \frac{1}{S_0} \left\langle \widehat{\phi_2}, f_0(k_0, z) \right\rangle - 1 \right| = \left| \frac{1}{S_0} \int_{-h_1}^{0} \widehat{\phi_2}, f_0(k_0, z) dz - 1 \right|, \quad \text{on } \Gamma_l, \tag{24}$$

$$K_t = |T_0| = \left| \frac{1}{S_0} \left\langle \widehat{\phi_2}, f_0(k_0, z) \right\rangle \right| = \left| \frac{1}{S_0} \int_{-h_1}^{0} \widehat{\phi_2}, f_0(k_0, z) dz \right|, \quad \text{on } \Gamma_r, \tag{25}$$

Also, the wave energy dissipation coefficient K_d is defined as:

$$K_d = \sqrt{1 - K_t^2 - K_r^2}, \tag{26}$$

2.3. Wave force on the VWBIC and oscillatory flow in the culvert

In this paper, the wave force on the upper structure of the VWBIC is calculated. It can be seen that the velocity potential ϕ of any point in the computational domain can be calculated by Eq. (17), and the normal derivative of the velocity potential $\frac{\partial \phi}{\partial n}$ can be obtained by ϕ. According to the linear wave theory, the pressure of any point in the computational domain can be expressed as:

$$-\frac{1}{\rho} P = \frac{\partial}{\partial t} \Phi \Rightarrow P = -\rho \frac{\partial}{\partial t} \Phi = \rho i \omega \phi, \tag{27}$$

The upper structure wave force $\boldsymbol{F}$ on the VWBIC can be expressed by integrating the pressure on the object surface Γ_{F3}

$$\boldsymbol{F} = (F_x, F_z) = \int_{\Gamma_{F3}} P \boldsymbol{n} d\Gamma, \tag{28}$$

where $\boldsymbol{n} = (n_x, n_z)$ is the unit normal vector of the object surface, F_x is the horizontal wave force and F_z is the vertical wave force.

According to the research of Lv and Zhao (2021), under the action of waves, an oscillatory flow will be produced in the culvert, which can promote the water exchange between the harbor area and the offshore area. Because the water satisfies the continuity condition, the oscillatory flow of any section in the culvert is the same. Therefore, the maximum oscillatory flow Q_m is defined as follows:

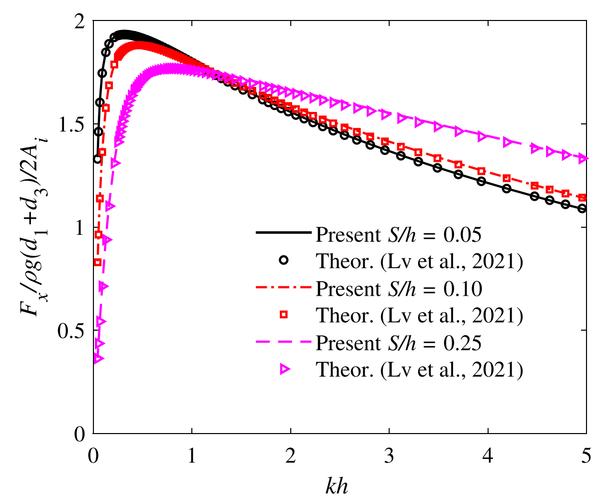

Fig. 5. Comparisons of horizontal wave force F_x between the present EEBEM results and theoretical solutions of Lv and Zhao (2021). $h_1 = h_2 = h$, $B/h = 1$, $d_n/h = 0.3$, $\theta = 0$, $L_p = 0$ m.

$$Q_m = \left| \left(\int_{-d_2}^{-d_1} \frac{\partial \phi_2}{\partial x} dz \bigg|_{x=-B} + \int_{-d_4}^{-d_3} \frac{\partial \phi_2}{\partial x} dz \bigg|_{x=B} \right)/2 \right|, \tag{29}$$

2.4. Verifications of the EEBEM

2.4.1. Convergence tests of the EEBEM

Since the number of expansion term M of velocity potential ϕ affects the precision of the model, it is necessary to select the appropriate expansion term M to guarantee the model accuracy and reduce the calculation time of the EEBEM. In the following calculations, Γ_l and Γ_r are located at a distance of $h_1/2$ from the VWBIC, and the boundary element length of each element is equal to dl. Fig. 3 shows the convergence tests of wave transmission coefficient K_t and relative difference R_d with different expansion terms M. R_d is defined as $R_d = |K_t(S) - K_t(M)|/K_t(S)$, where $K_t(M)$ is the wave transmission

Table 1
Convergence tests of K_t with different boundary element length dl (m). h_1 = 0.4 m, h_2 = 0.36 m, B = 0.2 m, S = 0.04 m, d_n = 0.2 m, θ = 20°, L_p = 0.16 m, $\epsilon = 0.8$, $m_p = 1$, $f_p = 0.2$, M = 10.

kh_1	Wave transmission coefficient K_t							
	$dl = 0.02$	0.01	0.005	0.004	0.0025	0.002	0.0015	0.001
0.02	0.9918	0.9920	0.9921	0.9921	0.9922	0.9922	0.9922	0.9922
0.50	0.3114	0.3134	0.3143	0.3144	0.3146	0.3147	0.3147	0.3147
1.00	0.1522	0.1531	0.1534	0.1535	0.1536	0.1536	0.1536	0.1536
1.50	0.0890	0.0893	0.0894	0.0894	0.0895	0.0895	0.0895	0.0895
2.00	0.0534	0.0533	0.0533	0.0533	0.0533	0.0533	0.0533	0.0533
2.50	0.0320	0.0317	0.0316	0.0316	0.0316	0.0316	0.0316	0.0316
3.00	0.0193	0.0188	0.0187	0.0186	0.0186	0.0186	0.0186	0.0186

coefficient with the expansion terms equal to M, and $K_t(S)$ represents the convergent wave transmission coefficient. It can be seen that when the expansion term $M = 4$, the results are convergent, and R_d is less than 0.1%. In addition, since the EEBEM model is a numerical model, it is crucial to choose the suitable boundary element length dl. Table 1 shows the convergence tests of K_t with different boundary element length dl. It is obvious that when $dl = 0.002$ m, the results are accurate to four decimal places. Therefore, the values of dl = 0.002 m and $M = 10$ are selected in the following calculations.

2.4.2. Validations of the EEBEM

To validate the present EEBEM model with the standard results of Lv and Zhao (2021), in Figs. 4 and 5, wave transmission, reflection coefficients K_t and K_r, maximum oscillatory flow Q_m and horizontal wave force F_x are plotted as a function with dimensionless wavelength kh. It is clearly seen that the present results agree well with those obtained by Lv and Zhao (2021), indicating that the present results are correct. In addition, to verify the correctness of the rubble mound foundation, the parameters of the rubble mound foundation are set as $\epsilon = 0, m_p = 1, f_p = 1000000$, which means the rubble mound foundation is impermeable. Fig. 6 displays the comparisons of wave transmission coefficient K_t between the present EEBEM results and theoretical solutions of Lv and Zhao (2021). It is found that the present results were basically consistent with the theoretical results, which indicates that the EEBEM model can better simulate the interaction between the wave and the VWBIC.

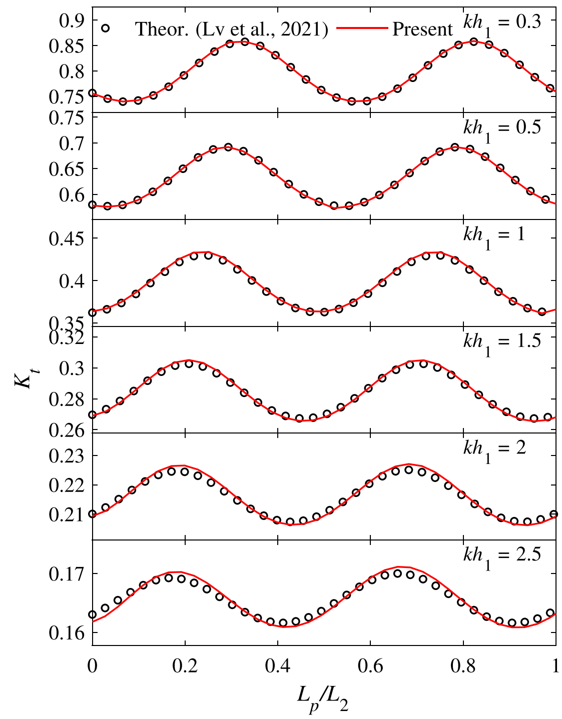

Fig. 6. Comparisons of wave transmission coefficient K_t between the present EEBEM results and theoretical solutions of Lv and Zhao (2021). $h_1 = 0.5$ m, $h_2 = 0.3$ m, $B = 0.25$ m, $d_n = 0.15$ m, $S = 0.1$ m, $\theta = 0°$, $\epsilon = 0, m_p = 1, f_p = 1000000$.

Table 2
Conditions of CFD numerical simulations.

Case	h (m)	B (m)	d_n (m)	S (m)	θ (°)	H_i (m)	T_i (s)
1–14	0.40	0.15	0.20	0.06	30.00	0.02, 0.06	0.9-3.0
15–28	0.40	0.15	0.20	0.06	−30.00	0.02, 0.06	0.9-3.0
29–35	0.40	0.15	0.20	0.06	15.00	0.02	0.9-3.0
36–42	0.40	0.15	0.20	0.06	0.00	0.02	0.9-3.0
43–49	0.40	0.15	0.20	0.08	30.00	0.02	0.9-3.0
50–56	0.40	0.15	0.20	0.04	30.00	0.02	0.9-3.0
57–63	0.40	0.20	0.20	0.06	30.00	0.02	0.9-3.0

Note: T_i = 0.9–3.0 means it can be selected as 0.90, 1.0, 1.2, 1.4, 2.0, 2.4, 3.0.

3. Computational fluid dynamics (CFD) numerical model

To reveal the mechanism of wave interaction with the VWBIC and further confirm the reliability of the EEBEM, computational fluid dynamics (CFD) simulations were used.

3.1. CFD model

A CFD model adopting volume-average/point-value method (VPM) is used to solve the Navier–Stokes equation based on the OpenFOAM (Xie et al., 2014; Zhang et al., 2019). The motion of incompressible fluid can be written as:

$$\nabla \cdot \boldsymbol{U} = 0, \tag{30}$$

$$\frac{\partial \rho \boldsymbol{U}}{\partial t} + \nabla \cdot (\rho \boldsymbol{U} \otimes \boldsymbol{U}) = -\nabla p + [\nabla \cdot (\mu \nabla \boldsymbol{U}) + \nabla \boldsymbol{U} \cdot \nabla \mu] + \boldsymbol{F}_\sigma - \boldsymbol{g} \cdot \mathbf{x} \nabla \rho, \tag{31}$$

$$\frac{\partial \alpha}{\partial t} + \boldsymbol{U} \cdot \nabla \alpha = 0, \tag{32}$$

where $\boldsymbol{U} = (u, v)$ is the fluid particle velocity; p is the relative dynamic pressure; ρ is the fluid density; μ is the dynamic viscosity coefficient; $\boldsymbol{g}$ is the acceleration of gravity; $\mathbf{x} = x, z$ is the coordinate point; $\boldsymbol{F}_\sigma$ is the surface tension and the expression is as follows

$$\boldsymbol{F}_\sigma = \sigma_t \kappa \nabla \alpha, \tag{33}$$

where σ_t is the tension coefficient; κ is the average curvature of the interface; α is the fluid volume fraction and $0 \le \alpha \le 1$. Then the fluid characteristics in the grid can be written as

$$\chi = \chi_1 \alpha + \chi_2 (1 - \alpha), \tag{34}$$

where χ is the density ρ or viscosity coefficient μ of the fluid in the grid.

Wave in the NWT is generated by the velocity boundary conditions, and relaxation method proposed by Jacobsen et al. (2012) is used to eliminate the secondary reflection wave.

Fig. 7 displays a diagram of CFD numerical wave tank (NWT). The NWT is 26 m long with the relaxation zone being 5 m and 8 m at the beginning and the end of the NWT, respectively. Five wave gauges, named WG1-WG5, are set up at 9.0 m, 9.3 m, 9.5 m, 16.5 m and 16.7 m, which are used to calculate the reflection and transmission coefficient by Goda's two-point method (Goda and Suzuki, 1976). Besides, to measure the maximum oscillatory flow Q_m in the culvert, three velocity section measurement points named GV1-GV3 are set at 14.0 m, 14.15 m and 14.3 m. Table 2 shows the conditions of CFD numerical simulations, in which the results of $H_i = 0.02$ m are used to compare with the EEBEM results, while the results of $H_i = 0.06$ m are used to reveal the mechanism of wave interaction with the VWBIC.

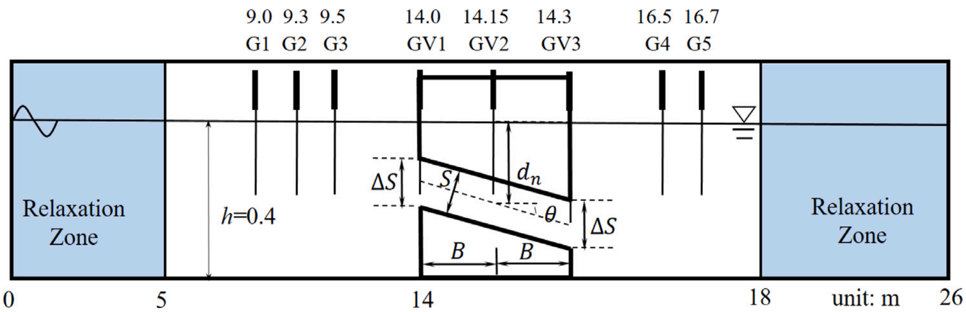

Fig. 7. Schematic diagram of a CFD numerical wave tank.

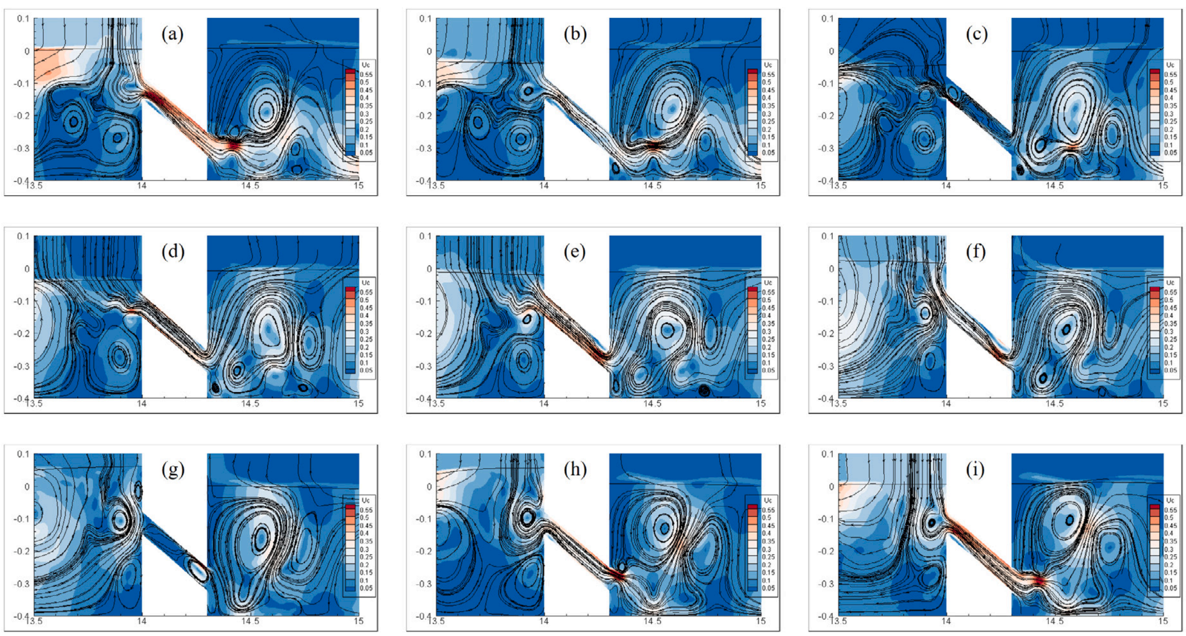

Fig. 8. Variations of wave surface and flow velocity fields in one period (through the CFD), and time interval is $T_i/8$. $h_1 = h_2 = 0.4$ m, $B = 0.15$ m, $d_n = 0.2$ m, $S = 0.06$ m, $\theta = 30°$, $L_p = 0$ m, $T_i = 2.4$ s, $H_i = 0.06$ m.

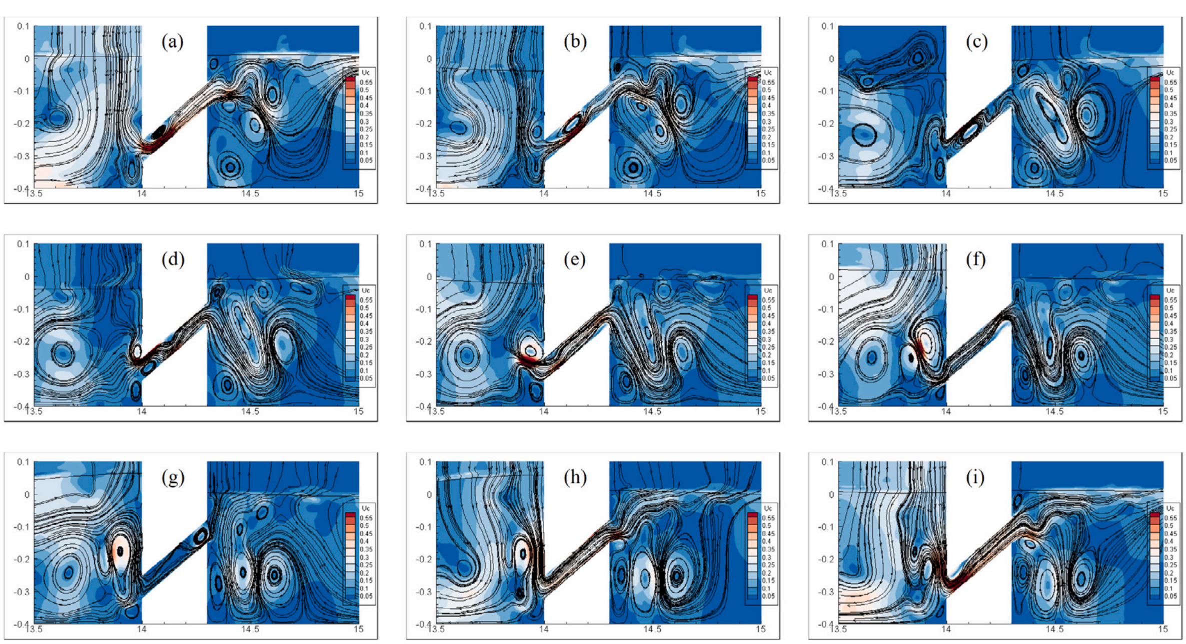

Fig. 9. Variations of wave surface and flow velocity fields in one period (through the CFD), and time interval is $T_i/8$. $h_1 = h_2 = 0.4$ m, $B = 0.15$ m, $d_n = 0.2$ m, $S = 0.06$ m, $\theta = -30°$, $L_p = 0$ m, $T_i = 2.4$ s, $H_i = 0.06$ m.

3.2. Flow fields of wave interaction with the VWBIC

Figs. 8 and 9 show the variations of wave surface and flow velocity fields in one period with different culvert inclined angle θ at 9 typical phases (time interval is $T_i/8$). For convenience of description, it is assumed that the fluid domain on the left side of the VWBIC is the sea area (with low sediment concentration) and the fluid domain on the right side is the harbor area (with high sediment concentration). Besides, the distribution of sediment concentration also follows the law of being sparse at the top and dense at the bottom.

As can be seen from Figs. 8 and 9, under the action of waves, a high-speed oscillatory flow will be formed in the culvert, and the streamline of the oscillatory flow is basically parallel to the culvert direction. When the wave surface is close to the mean sea level, the velocity in the culvert reaches its maximum. In addition, the vortexes generated by the interaction between the wave and the VWBIC are mainly distributed near the culvert, and its velocity is relatively low.

Fig. 8 shows that when the culvert inclined angle θ is positive, within half a period of the incident wave moving from the trough to the crest (Fig. 8(c–g)), high turbidity water in the culvert and the harbor area is gradually brought into the sea area. Meanwhile, a vortex is generated under the culvert inlet. When the water in the harbor area is brought to the vicinity of the culvert inlet, this vortex can further diffuse and promote water exchange. Similarly, within half a period of the incident wave moving from the crest to the trough (Fig. 8(g–c)), low turbidity water in the culvert and sea area is gradually brought into the harbor area. At the same time, a high velocity zone near the culvert outlet will gradually move to the interior of the harbor area, which can move about one VWBIC's length in half a period. In this process, the oscillatory flow is used to transport the water, while the vortex and turbulence are used to diffuse the water. Then, the high turbidity water is fully mixed and exchanged with the low turbidity water under the synergistic action of oscillatory flow, vortex and turbulence.

Fig. 9 represents a variation corresponding to Fig. 8. It is found that the phenomenon of $\theta = 30°$ is basically consistent with that of $\theta = -30°$. The difference is that there will be some small vortexes in the culvert, which will reduce the velocity of the oscillatory flow and weaken the effect of water exchange. Besides, due to the effects of sediment distribution, the effect of sediment exchange of $\theta = -30°$ is weaker than that of $\theta = 30°$ when the oscillatory flow is the same.

In fact, under the linear wave theory, the oscillatory flow increases linearly with the increase of the wave height, so the effect of water exchange can be improved with the increase of wave height. In addition, Lv and Zhao (2021) found that with the increase of the wave nonlinearity, a net mass transport flow similar to Stokes drift will appear in the culvert, which can further promote water exchange. Therefore, although the water exchange capacity in one wave period is not large, the effect of water exchange will gradually expand under the action of waves for a long time due to the synergistic effect of the oscillatory flow, vortex and turbulence. This indicates that the VWBIC can reduce sediment deposition in the harbor basin and improve the living environment of organisms.

3.3. Comparisons of the CFD and EEBEM

Fig. 10 represents the comparisons of wave transmission coefficient K_t, reflection coefficient K_r, energy dissipation coefficient K_d and maximum oscillatory flow Q_m as a function of the relative water depth kh between the EEBEM and CFD results. As shown in Fig. 10, K_t and Q_m of the CFD and EEBEM results are in good agreement, and K_r of the CFD results are slightly smaller than that of the EEBEM. In the CFD simulations, the maximum value of K_d is 0.14 when $kh = 0.44$, and the energy dissipation tends to decrease with the increase of kh. In fact, the energy dissipation is caused by the synergistic effect of the oscillatory flow, vortex, and turbulence. The velocity of the oscillatory flow, vortex and turbulence increase with the increase of wavelength, which makes the energy dissipation of long waves greater than that of short waves. However, in the actual ocean, such as the East China Sea, waves are concentrated in the interval of $2.5 > kh > 0.5$, and the occurrence probability of long wave is relatively small. Therefore, it can be considered that the energy dissipation caused by the interaction between waves and the VWBIC is very small and negligible.

Besides, when the culvert inclined angle θ is opposite, such as $\theta = 30°$ and $\theta = -30°$, both the amplitude of the transmission wave and reflection wave are the same, while the oscillatory flow with positive inclined angle ($+\theta$) is obviously larger than that with negative inclined angle ($-\theta$). When the relative water depth kh is greater than 0.5, the maximum oscillatory flow Q_m of $\theta = 30°$ is gradually larger than that of $\theta = -30°$, and this phenomenon becomes more obvious with the increase of kh. This result means the VWBIC is more beneficial to practical application when the culvert inclined angle is positive, and this phenomenon has great significances to practical engineering. The above phenomena can be explained as follows: the velocity potential near the VWBIC can be divided into wave propagation mode and evanescent mode. The propagation mode is only related to the integral of Green's function, and will not be changed because the integral of Green's function is constant (when the distance from the VWBIC is large enough, the evanescent mode is equal to 0). Furthermore, Kashiwagi and Hayashi (2008) also proved that for the diffraction problem of asymmetric floating structures, the amplitudes of transmission wave and reflection wave are the same, regardless of the incident direction of incident wave. But for the maximum oscillatory flow Q_m, it is related to both the propagation mode and evanescent mode. Although the propagation mode is constant, when the distance of the culvert inlet is close to the wave surface, the evanescent mode will be bigger, and the oscillatory flow will be larger.

Fig. 11 shows the comparisons of wave transmission coefficients K_t, reflection coefficient K_r, and maximum oscillatory flow Q_m between the EEBEM and CFD results under the condition of $H_i = 0.02$ m. It is obvious that the EEBEM results and CFD results are in good agreement in different conditions. When the incident wave is linear ($H_i = 0.02$ m) and the wavelength is small (K_t and Q_m are small, and K_r is large), the results of the EEBEM and CFD are basically consistent. With the increase of wavelength (K_t and Q_m become larger, and K_r becomes smaller), CFD results gradually deviate from the EEBEM results. However, the differences between the EEBEM and CFD results are small, which further indicates that energy dissipation caused by the interaction between waves and the VWBIC is small, and the EEBEM based on the linear potential flow theory can better simulate the interaction between waves and the VWBIC.

4. Results and discussion

4.1. The effects of the culvert inclined angle

As described in Section 3.3, different incident wave directions (same θ with the opposite sign) do not cause the change of wave transmission and reflection coefficients, but have a great influence on the oscillatory flow. When the culvert inclined angle is positive, the structure is more beneficial to practical application. Therefore, in the following analysis, only the positive inclined angle is analyzed, namely, the culvert inlet is close to the water surface and the outlet is close to the bottom. In addition, the culvert length B is mainly designed with the wave force to ensure the stability of the structure, and it cannot be easily changed. Culvert height S and culvert depth d_n are the most important factors affecting water exchange for the encircled harbor basin. Thereby, to make the following calculations more representative, the optimal culvert parameters proposed by Lv and Zhao (2021) are adopted as the basic calculation parameters ($B/h = 0.3, S/h = 0.275, d_n/h = 0.8$), when the effect of the inclined angle is analyzed.

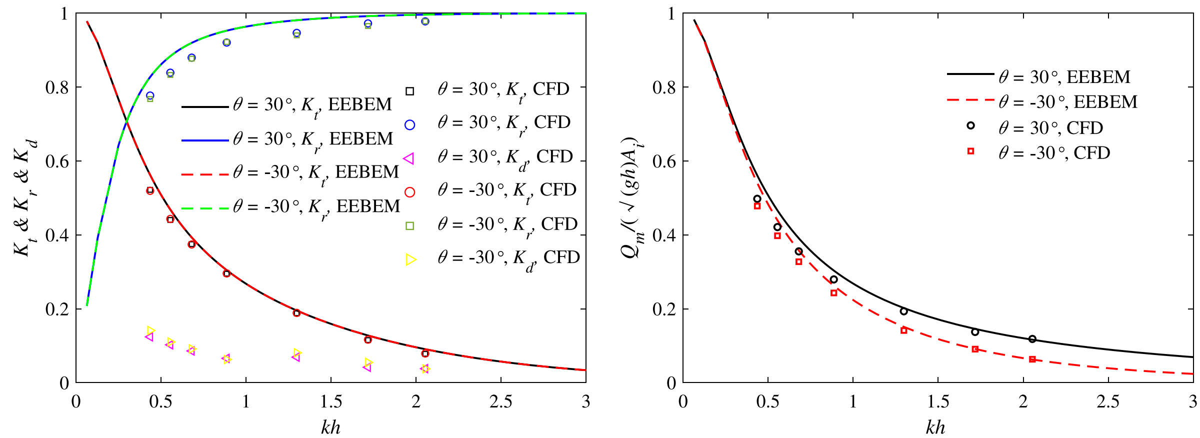

(a) Wave transmission coefficient K_t, reflection coefficient K_r and energy dissipation coefficient K_d

(b) Maximum oscillatory flow Q_m

Fig. 10. Comparisons of K_t, K_r, K_d, and Q_m between the EEBEM results and CFD numerical results. $h_1 = h_2 = 0.4$ m, $B = 0.15$ m, $d_n = 0.2$ m, $S = 0.06$ m, $L_p = 0$ m, $H_i = 0.02$ m.

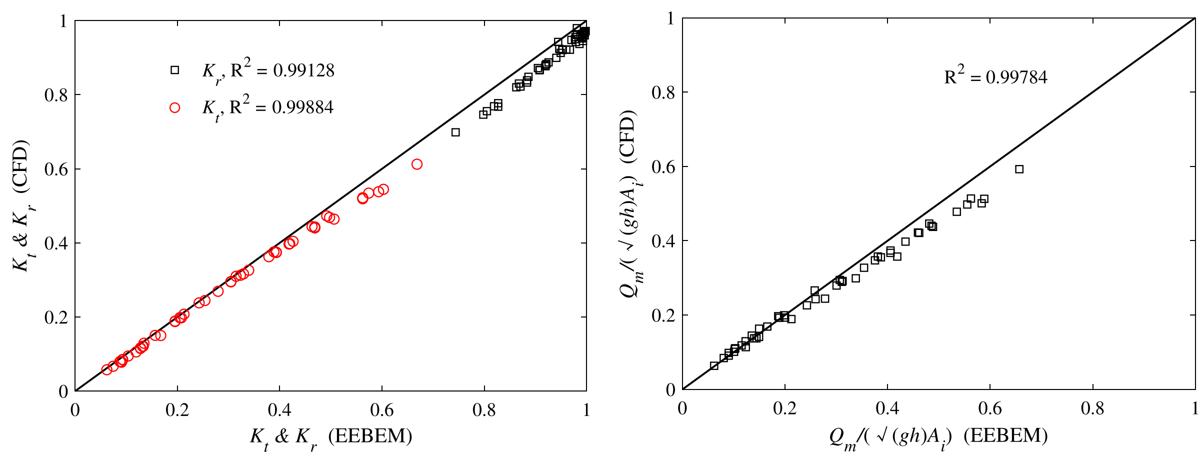

(a) Wave transmission coefficient K_t and reflection coefficient K_r

(b) Maximum oscillatory flow Q_m

Fig. 11. Comparisons of K_t, K_r and Q_m between the EEBEM results and CFD numerical results under the condition of $H_i = 0.02$ m (for Table 2).

4.1.1. When the culvert inlet height is constant

To find the effects of the culvert inclined angle θ on the hydrodynamic performance of the VWBIC when the culvert inlet height ΔS is constant, assuming that the position of the culvert outlet d_4 and the culvert inlet height remained unchanged. The change of θ is accomplished by adjusting the distance between the culvert inlet and the still water level. Fig. 12 displays the variations of the wave transmission and reflection coefficients K_t and K_r (Fig. 12(a)), maximum oscillatory flow Q_m (Fig. 12(b)), horizontal wave force F_x (Fig. 12(c)) and vertical wave force F_z (Fig. 12(d)) as a function of the dimensionless wavelength kh for different culvert inclined angle ($\theta = 0°, 14.04°, 26.57°, 36.87°$). Figs. 13 and 14 represent the variations corresponding to Fig. 12 for different culvert inlet heights ($\Delta S/h = 0.15$ and 0.05).

When the wave transmission coefficient K_t of $\theta > 0°$ is equal to the value of $\theta = 0°$, the corresponding kh is defined as a critical wavelength. In Fig. 12(a) and (b), it is found that when kh is larger than the critical wavelength, K_t and Q_m obviously increase with the increase of θ. When kh is smaller than the critical wavelength, K_t and Q_m decrease slightly with the increase of θ. As the probability of long waves and short waves appearing in the ocean is low, if the critical wavelength decreases, the effects of wave elimination and water exchange will be enhanced. Fig. 12(c) displays that the peak value of F_x drops sharply with the increase of θ, and the value of kh matching with the peak value of F_x is almost unchanged. In Fig. 12(d), it can be found that, when $\theta = 0°$, the peak value of $F_z/\rho g2BA_i$ appears at $kh = 0$ and the value is equal to 1. With the increase of θ, the peak value of $F_z/\rho g2BA_i$ increases gradually, and the value of kh matching with the peak value also increases slightly. It can be seen from the above that the hydrodynamic performance of the inclined culvert is better than that of the horizontal culvert ($\theta = 0°$).

The variation tendencies of Figs. 13 and 14 are almost the same as those in Fig. 12. By comparing Figs. 12, 13 with 14, it can be found that with the decrease of culvert inlet height $\Delta S/h$, the critical wavelength and the peak value of F_x gradually increases. It is easy to know that these phenomena are not constructive to the optimal design of the VWBIC. Therefore, in practice, choosing a larger culvert inlet height and culvert inclined angle are extremely important, so as to make the effects of VWBIC on wave elimination and water exchange stronger, as well as make the structure more stable.

4.1.2. When the culvert height is constant

To find the effects of the culvert inclined angle on the hydrodynamic performance of the VWBIC when the culvert height S is constant,

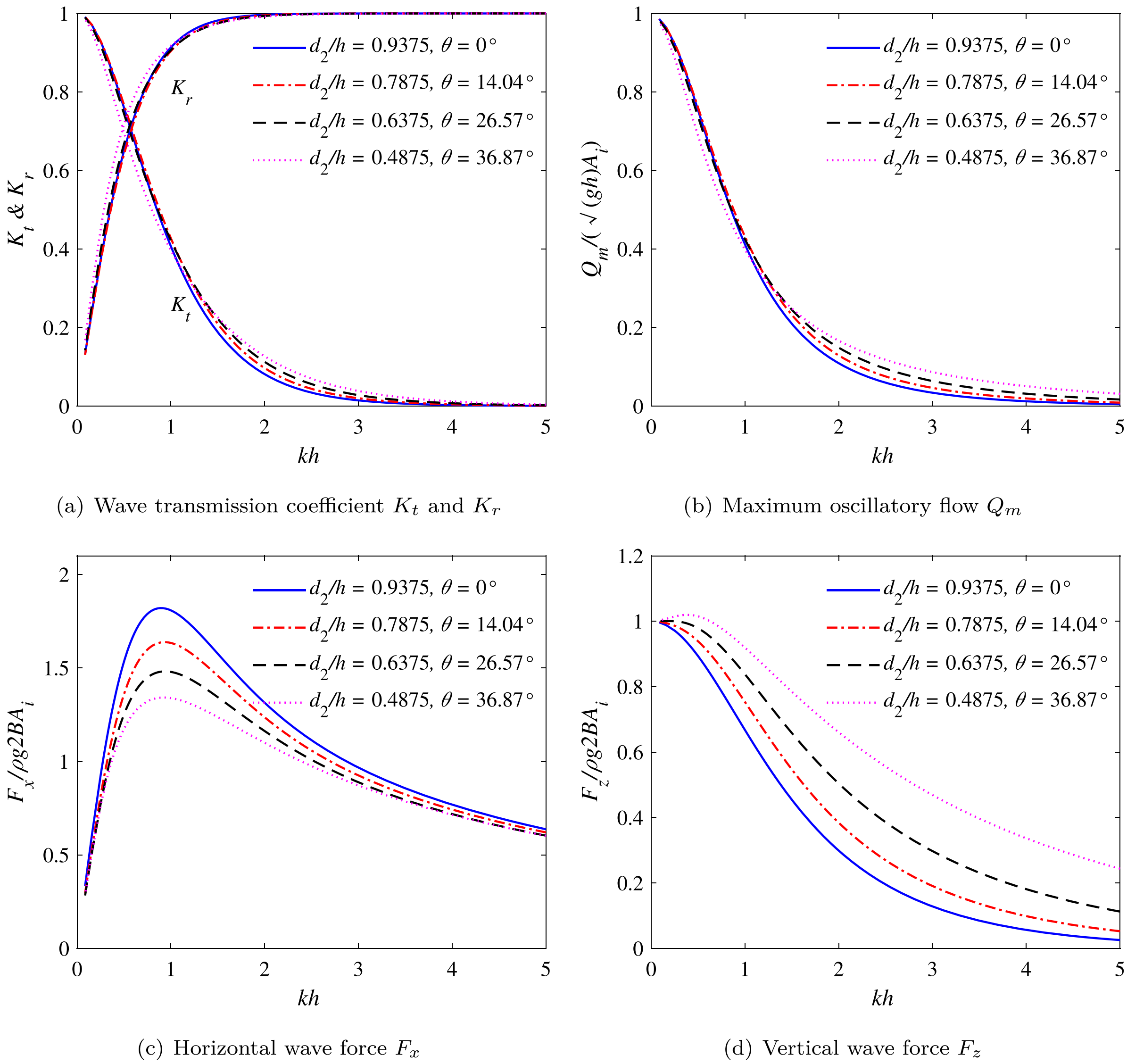

(a) Wave transmission coefficient K_t and K_r

(b) Maximum oscillatory flow Q_m

(c) Horizontal wave force F_x

(d) Vertical wave force F_z

Fig. 12. When the culvert entrance height ΔS is constant, K_t, K_r, Q_m, F_x and F_z as a function of dimensionless wavelength kh for different culvert inclined angles θ (through the EEBEM). $h_1 = h_2 = h$, $B/h = 0.3$, $d_3/h = 0.6625$, $d_4/h = 0.9375$, $\Delta S/h = 0.275$, $L_p/h = 0$.

assuming that the midpoint of the culvert outlet $(d_3 + d_4)/2$ and S remained unchanged. When S is constant, Fig. 15 shows the variations of the wave transmission and reflection coefficients K_t and K_r (Fig. 15(a)), maximum oscillatory flow Q_m (Fig. 15(b)), horizontal wave force F_x (Fig. 15(c)) and vertical wave force F_z (Fig. 15(d)) as a function of the dimensionless wavelength kh for different culvert inclined angle ($\theta = 0°, 18.43°, 33, 69°, 45°$). As can be seen from the figure, the trends of Figs. 15 and 12 are basically the same, but there are still some differences between them.

It is observed from Fig. 15(a) and (b) that θ has few effects on K_t, K_r and Q_m when $kh < 0.5$. With the increase of kh, the differences of K_t and Q_m between different θ become larger. This is because the vertical energy distribution of water with different wavelengths is different. The greater the culvert inclined angle, the closer the culvert inlet is to the water surface. Then more wave energy can pass through the culvert, which results in the increase of K_t and Q_{tm}. In addition, the critical wavelength does not exist in Fig. 15, which means that when $\theta > 0$, the corresponding value of K_t and Q_{tm} is greater than that when $\theta = 0$. Therefore, in practical application, as K_t and Q_{tm} increase with the increase of θ, the effects of culvert inclined angle θ still needs to be further evaluated when the culvert height is constant. For more details, please refer to Section 4.3. In Fig. 15(c), the peak value of $F_x/\rho g2BA_i$ = 1.05 when $\theta = 45°$, and the peak value of $F_x/\rho g2BA_i = 1.82$ when $\theta = 0°$, which means the peak value of F_x sharply decrease with the increase of θ. In Fig. 15(d), the peak value of F_z is almost unchanged and the maximum value of $F_z/\rho g2BA_i$ is approximately equal to 1 for different θ. Therefore, considering the phenomenon of wave force, increasing the culvert inclined angle can effectively improve the stability of the VWBIC.

4.2. The effects of the permeable rubble mound foundation

According to the study of Lv and Zhao (2021), when the length and height of the impermeable rubble mound foundation are appropriate, wave transmission coefficient of spectra peak frequency can reach its minimum value due to the wave shoaling and wave resonance. In view of the fact that energy dissipation cannot be taken into account in the impermeable rubble mound foundation, this paper carries out the influences of permeable rubble mound foundation on wave hydrodynamics performance. For convenience of description, in this chapter, L_1 is linear wavelength when the water depth is h_1; k is the incident wavenumber when the water depth is h_1, and L_2 is linear wavelength when the water depth is h_2.

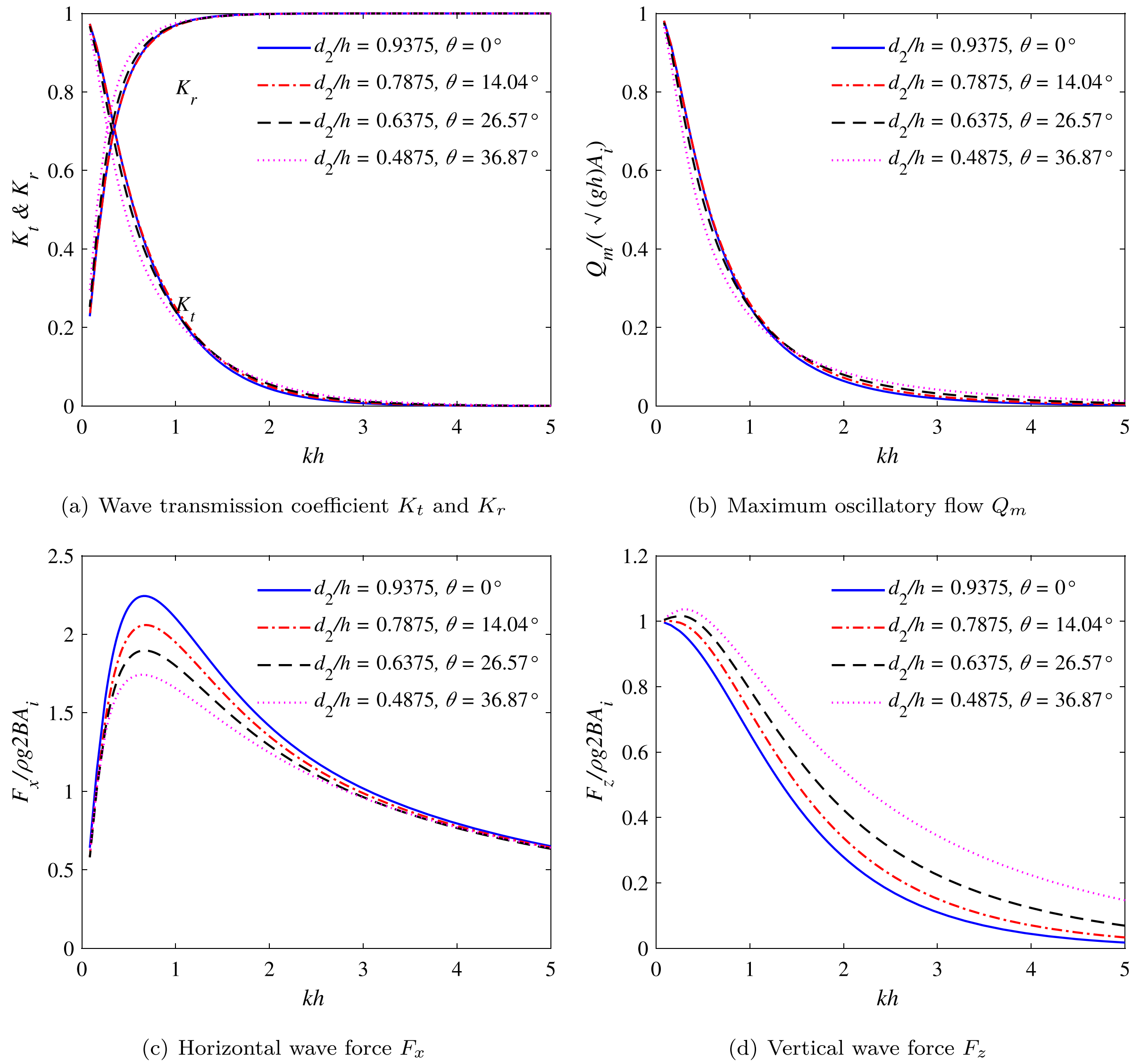

(a) Wave transmission coefficient K_t and K_r

(b) Maximum oscillatory flow Q_m

(c) Horizontal wave force F_x

(d) Vertical wave force F_z

Fig. 13. When the culvert entrance height ΔS is constant, K_t, K_r, Q_m, F_x and F_z as a function of dimensionless wavelength kh for different culvert inclined angles θ (through the EEBEM). $h_1 = h_2 = h$, $B/h = 0.3$, $d_3/h = 0.7875$, $d_4/h = 0.9375$, $\Delta S/h = 0.15$, $L_p/h = 0$.

4.2.1. The effects of the geometric parameters

To reflect the effects of the permeable rubble mound foundation more realistically, choosing appropriate values of three parameters porosity ε, inertial coefficient m_p and friction coefficient f_p is very important. According to Zhao et al. (2016) and Pérez-Romero et al. (2009), the inertial coefficient m_p can be assumed as 1, and the friction coefficient f_p can be calculated as:

$$f_p = 0.47(D_S k)^{-0.57}, \tag{35}$$

where D_S is the nominal diameter of stones, and k is the wavenumber. Considering the previous results of Zhao et al. (2016) and Pérez-Romero et al. (2009), $m_p = 1, f_p = 2, \varepsilon = 0.4$ was chose in the following calculations.

Fig. 16 represents the variations of wave transmission coefficient K_t, reflection coefficient K_r and energy dissipation coefficient K_d with relative length (L_p/L_1) and relative height $(1 - h_2/h_1)$ of the rubble mound foundation (through EEBEM). It is observed that, unlike the impermeable rubble mound foundation (refer to Lv and Zhao (2021) Fig. 17), except the phenomenon of wave shoaling and wave resonance, due to the energy dissipation caused by the permeable rubble mound foundation, K_t, K_r and K_d generally show a significant downward trend with the increase of the rubble mound foundation's length and height. The influence of permeable rubble mound foundation on K_r and K_d is much greater than K_t. For example, when $kh = 0.5$, K_r changes from 0.8 to 0.1, and K_d changes from 0.8 to 0 while K_t changes from 0.6 to 0.35. Similarly, when $kh = 1.5$, K_r decreases from 0.93 to 0.4, K_d changes from 0.8 to 0, and K_t decreases from 0.28 to 0.27. However, it should be noted that in practical application, the length of the rubble mound foundation is generally equivalent to the water depth. Therefore, permeable rubble mound foundation has few influences on the long waves, and is mainly used to eliminate the energy of medium waves and short waves and reduce the reflection in front of the breakwater.

Due to the complexity of the interaction among the wave resonance, wave shallowing and energy dissipation, in order to intuitively understand the effects of the rubble mound foundation on hydrodynamic performance of the VWBIC, Fig. 17 shows the variations of transmission coefficient K_t, reflection coefficient K_r, and energy dissipation coefficient K_d against relative length of the rubble mound foundation L_p/L_2. As can be seen from the figure, with the increase of L_p/L_2, K_t, K_r and K_d show the characteristics of periodic oscillation. The oscillation curve can be regarded as the superposition of a straight line and periodic function with an oscillation period of $L_2/2$. Compared with Fig. 18

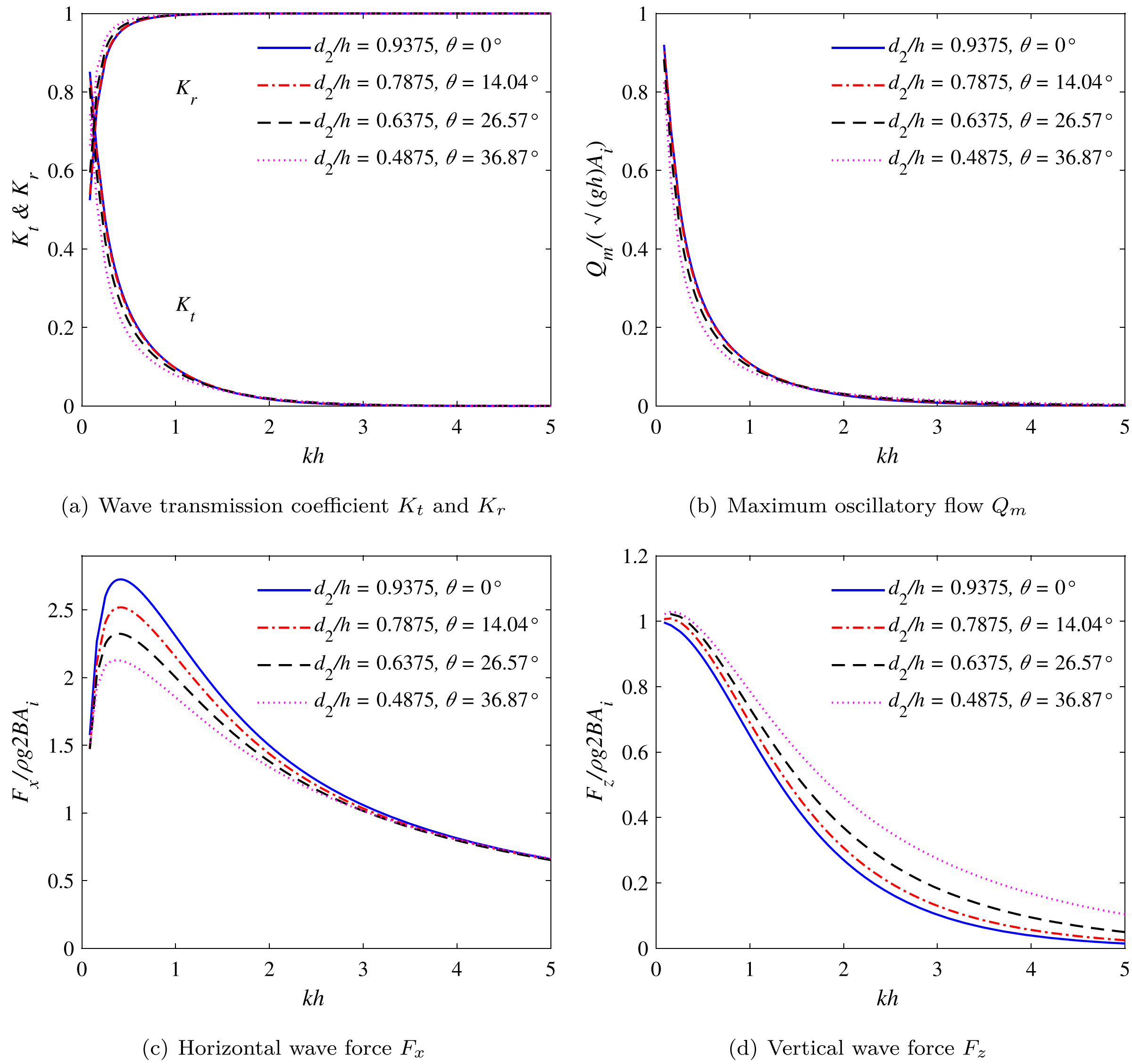

(a) Wave transmission coefficient K_t and K_r (b) Maximum oscillatory flow Q_m

(c) Horizontal wave force F_x (d) Vertical wave force F_z

Fig. 14. When the culvert entrance height ΔS is constant, K_t, K_r, Q_m, F_x and F_z as a function of dimensionless wavelength kh for different culvert inclined angles θ (through the EEBEM). $h_1 = h_2 = h$, $B/h = 0.3$, $d_3/h = 0.8875$, $d_4/h = 0.9375$, $\Delta S/h = 0.05$, $L_p/h = 0$.

of Lv and Zhao (2021), it can be considered that the straight line is caused by energy dissipation, while the periodic curve is caused by the wave resonance and shallowing. Besides, Fig. 17 displays that when $L_p = L_2/4 + L_2/2 * n$ ($n = 0, 1, 2\ldots$), K_d reaches the maximum value, K_r reaches the minimum value and K_t is equal to the node value of the periodic function. This means that K_t is hardly affected by wave resonance and wave shallowing, when K_r and K_d are in resonance. In practical applications, it is necessary to minimize the reflection of some waves to ensure the stability of the breakwater. It can be seen from the above that setting an appropriate length of the rubble mound foundation ($L_p = L_2/4 + L_2/2 * n$) can significantly reduce the reflection coefficient of the most important wave.

4.2.2. The effects of the permeable parameters

Next, the sensitivity analysis of the rubble mound foundation's parameters ε, m_p and f_p are carried out. For the convenience of analysis, when the sensitivity of one parameter is analyzed, it is assumed that the other two parameters are unchanged. Actually, it should be noted that, according to the research of Sollitt and Cross (1973), f_p is highly correlated with ε. Changing ε will significantly change f_p. However, in this paper, the sensitivity of the corresponding parameters to the hydrodynamic characteristics of the structure is considered more, so the coupling relationship between them is not considered. In addition, f_p is a generalized parameter after linearization, which is affected by many parameters besides porosity, such as structural permeability, relative diameter, turbulent friction coefficient and the intrinsic permeability (Sollitt and Cross, 1973; Dalrymple et al., 1991; Pérez-Romero et al., 2009). According to the research of Dalrymple et al. (1991), f_p is close to $o(1)$. Therefore, it is meaningful to independently consider the influence of f_p and ε on the hydrodynamic performance of VWBIC.

Fig. 18 represents the effects of the rubble mound foundation's porosity ε on the wave transmission coefficient K_t, reflection coefficient K_r and energy dissipation coefficient K_d, horizontal wave force F_x and vertical wave force F_z. Figs. 19 and 20 demonstrate the variations of inertial coefficient m_p and friction coefficient f_p of the rubble mound foundation corresponding to Fig. 18. It can be seen from Fig. 18(a) that with the increase of ε, K_d increases, K_r and K_t decreases, and maximum energy loss occurs in $kh = 1.8$. This is because the wavelength L_2 on the rubble mound foundation is 1.6 m, which is 4 times as long as the rubble mound foundation's length 0.4 m, meeting the wave resonance condition. In addition, there is a small peak when kh is small. This is because the relative length of the rubble mound foundation (L_p/L_1) is too small, and the couple interaction between the wave initial phase and energy loss will produce a peak value. In Fig. 18(b), F_x and F_z

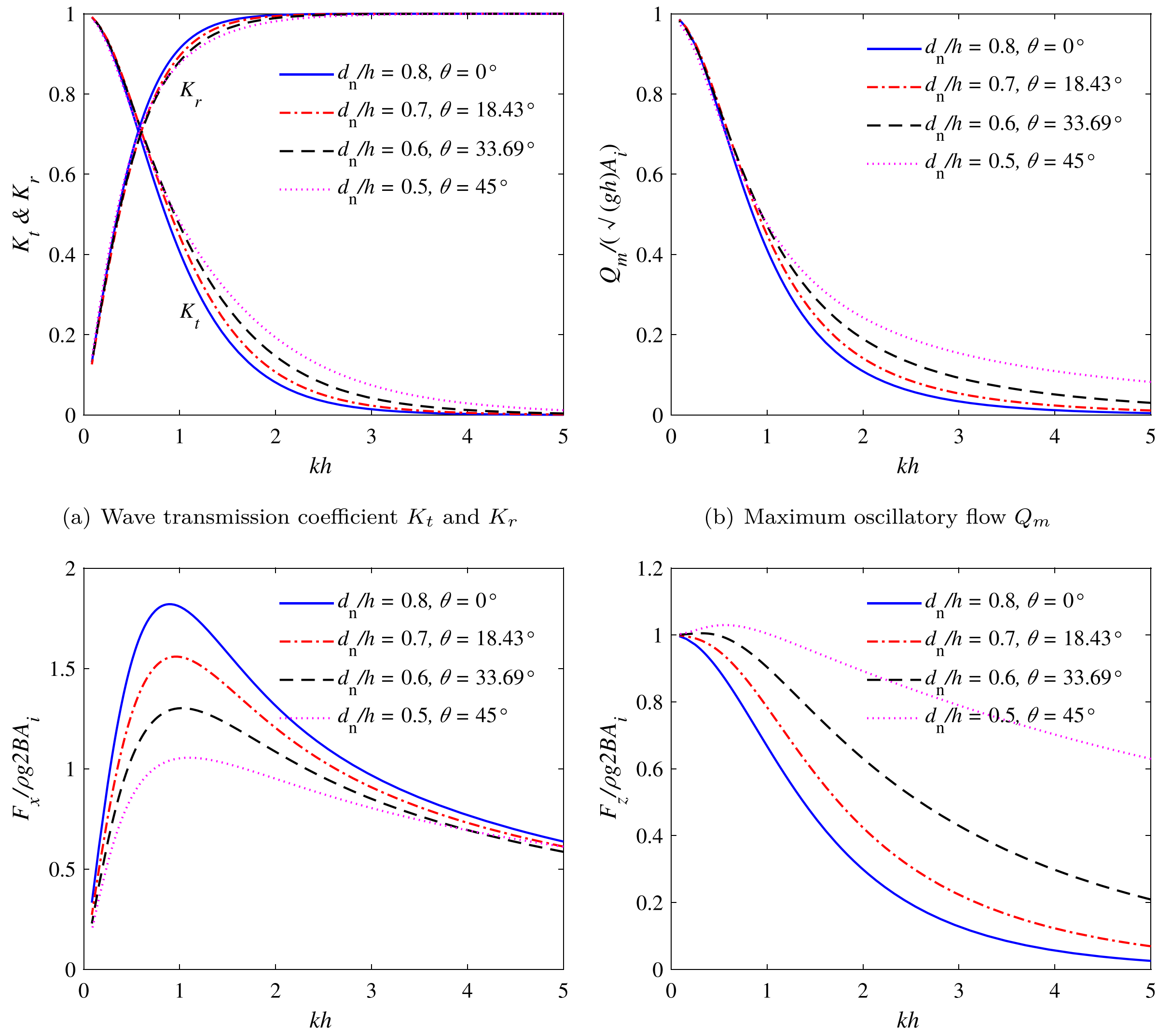

(a) Wave transmission coefficient K_t and K_r

(b) Maximum oscillatory flow Q_m

(c) Horizontal wave force F_x

(d) Vertical wave force F_z

Fig. 15. When the culvert height S is constant, K_t, K_r, Q_m, F_x and F_z as a function of dimensionless wavelength kh for different culvert inclined angles θ (through the EEBEM). $h_1 = h_2 = h$, $B/h = 0.3$, $S/h = 0.275$, $(d_3 + d_4)/2/h = 0.8$, $L_p/h = 0$.

decrease with the increase of ε, which indicates that the rubble mound foundation can reduce the wave force acting on the VWBIC to some extent. The variation rules of K_t, K_r, K_d, F_x and F_z with relative water depth of kh in Figs. 19 and 20 are basically the same as those in Fig. 18. In Fig. 19, it can be found that with the increase of inertial coefficient m_p, K_d decreases, while F_x and F_z slightly increase. Fig. 20 shows that with the increase of friction coefficient f_p, K_d first increases and then decreases.

The above results show that permeable rubble mound foundation can effectively dissipate the wave energy, reduce the reflection coefficient and wave force of the VWBIC, and maintain the stability of the structure. Especially, if the rubble mound foundation is under the condition of resonance, wave reflection coefficient of the peak frequency will reach its minimum value, which can improve the wave stability in the harbor area.

4.3. Optimization of the inclined culvert

Improving the ability of water exchange and berthing stability are the two main functions of the VWBIC, but the variation trend of the oscillatory flow (water exchange) and wave transmission coefficient (berthing stability) is similar. As a result, the optimization of the inclined culvert is to select appropriate parameters of the culvert, to make the wave transmission coefficient small while the oscillatory flow is large. In this paper, an optimal culvert calculation method which can comprehensively consider these two factors proposed by Lv and Zhao (2021) is used to judge the influence of the inclined culvert. The calculation method is briefly described as follows.

$$J_{Ki} = \begin{cases} (1-K_{ti})/(1-K_{tj}), & K_{ti} \geq K_{tj} \\ 1, & K_{ti} < K_{tj} \end{cases},$$
$$J_{Qi} = \begin{cases} 1, & Q_{mi} \geq Q_{tj} \\ Q_{mi}/Q_{tj}, & Q_{mi} < Q_{tj} \end{cases}. \quad (36)$$

where J_{Ki} is the evaluation value of wave transmission and J_{Qi} is the evaluation value of water exchange. K_{ti} is the wave transmission coefficient, K_{tj} is the critical wave transmission coefficient and $K_{tj} = 0.1$. Q_{mi} is the maximum oscillatory flow, Q_{tj} is the critical maximum oscillatory flow and $Q_{tj} = \sqrt{gh}A_i$.

The comprehensive evaluation value J_i of monochromatic wave is written as Eq. (37)

$$J_i = aJ_{Ki} + bJ_{Qi}, \quad (37)$$

where a, b is the weight factor and $a = b = 1$ is used in this paper.

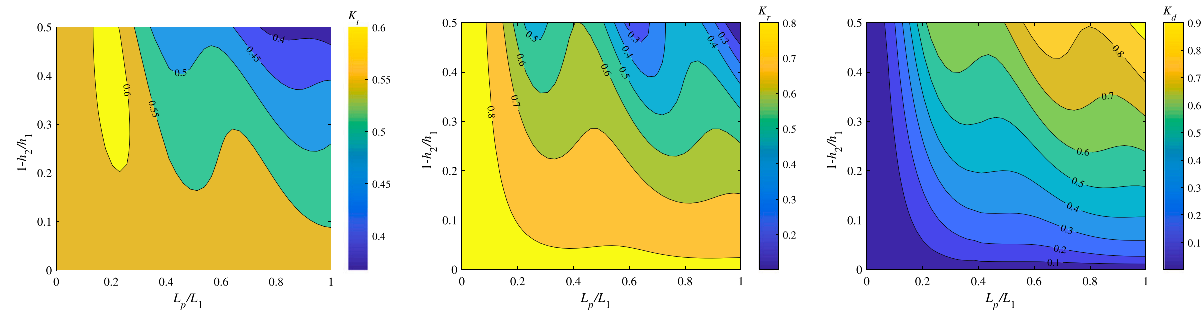

(a) Wave transmission coefficient K_t, $kh_1 = 0.5$

(b) Wave reflection coefficient K_r, $kh_1 = 0.5$

(c) Energy dissipation coefficient K_d, $kh_1 = 0.5$

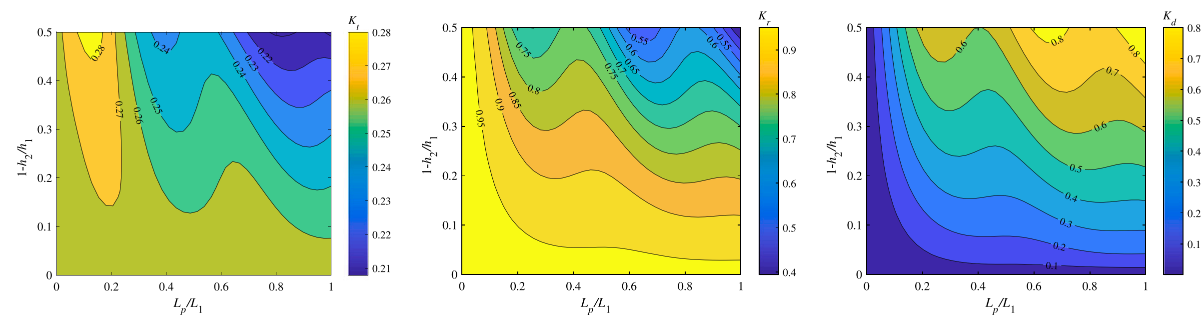

(d) Wave transmission coefficient K_t, $kh_1 = 1.5$

(e) Wave reflection coefficient K_r, $kh_1 = 1.5$

(f) Energy dissipation coefficient K_d, $kh_1 = 1.5$

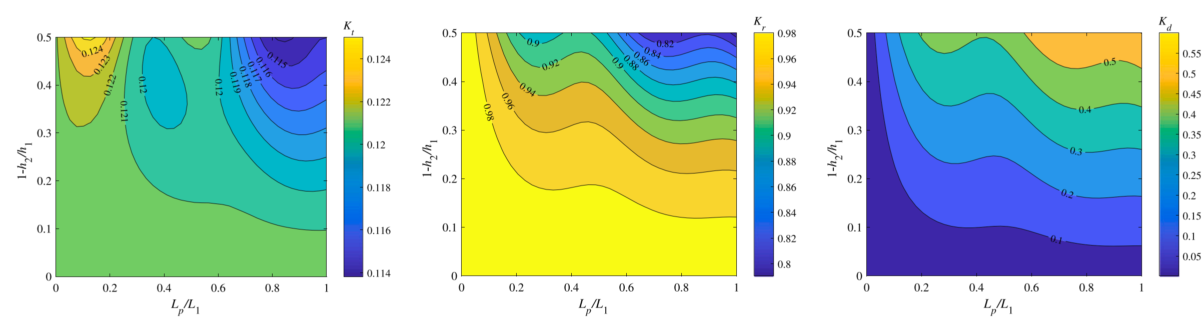

(g) Wave transmission coefficient K_t, $kh_1 = 3.0$

(h) Wave reflection coefficient K_r, $kh_1 = 3.0$

(i) Energy dissipation coefficient K_d, $kh_1 = 3.0$

Fig. 16. Variations of K_t, K_r and K_d with the length (L_p) and height ($h_1 - h_2$) of rubble mound foundation (through the EEBEM). $h_1 = h_3 = 0.5$ m, $B = 0.25$ m, $d_S = 0.15$ m, $S = 0.1$ m, $\theta = 0°$, $\varepsilon = 0.4$, $m_p = 1$, $f_p = 2$.

In the ocean, wave transmission evaluation value J_K, water exchange evaluation value J_Q and comprehensive evaluation value J of random waves can be written as Eq. (38)

$$J_K = \frac{\sum_{i=1}^{N} J_{Ki} \cdot S(f_i) \cdot df}{\sum_{i=1}^{N} S(f_i) \cdot df}, \quad J_Q = \frac{\sum_{i=1}^{N} J_{Qi} \cdot S(f_i) \cdot df}{\sum_{i=1}^{N} S(f_i) \cdot df},$$
$$J = \frac{\sum_{i=1}^{N} J_i \cdot S(f_i) \cdot df}{\sum_{i=1}^{N} S(f_i) \cdot df}, \tag{38}$$

In the following calculations, assuming that wave spectral density function $S(f)$ satisfies the joint north sea wave project (JONSWAP) spectrum

$$S(f) = \beta H_{1/3}^2 T_{ps}^{-4} f^{-5} \exp[-1.25(T_{ps} f)^{-4}] \gamma^{\exp[-(f/f_{ps}-1)^2/2\sigma^2]}, \tag{39}$$

$$\beta = \frac{0.06238(1.094 - 0.01915 \ln \gamma)}{0.230 + 0.0336\gamma - 0.185(1.9 + \gamma)^{-1}}, \tag{40}$$

where f_{ps} is the spectral peak frequency and T_{ps} is the spectral peak period. In the following calculations, significant wave height $H_{1/3} = 0.04$ m; water depth $h = 0.4$ m; $\gamma = 3.3$; $\sigma = 0.07 (f < f_{ps})$; $\sigma = 0.09 (f > f_{ps})$; the range of frequency f is from 0.40 Hz to 1.8 Hz; spectral peak frequency $f_{ps} = 0.8$ Hz and the number of constituent waves $N = 50$.

For different culvert structural parameters, when the comprehensive evaluation value J is the maximum value, the corresponding culvert can be regarded as the optimal solution, and the engineering application value of the VWBIC is the greatest. Fig. 21 displays the variations of the wave transmission evaluation value J_K, water exchange evaluation value J_Q and comprehensive evaluation value J with the change of the culvert inclined angle θ. In Fig. 21(a), when the culvert height S is constant, increasing the culvert inclined angle can effectively optimize the hydrodynamics performance of the VWBIC. When the inclination is the same, J_K of θ and $-\theta$ is the same. When $\theta < 0$, increasing θ has few effects on J_Q, but when $\theta > 0$, increasing θ can significantly improve the value of J_Q. In Fig. 21(b), when the culvert inlet height ΔS is constant

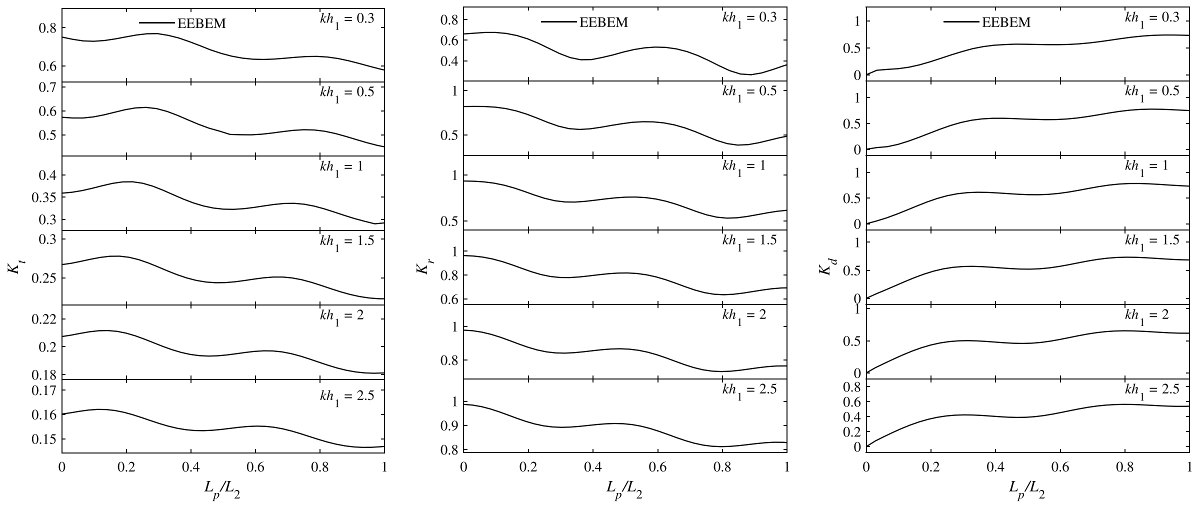

(a) Wave transmission coefficient K_t (b) Wave reflection coefficient K_r (c) Energy dissipation coefficient K_d

Fig. 17. Variations of K_t, K_r and K_d with the length (L_p) of rubble mound foundation (through the EEBEM). $h_1 = 0.5$ m, $h_2 = 0.3$ m, $B = 0.25$ m, $d_n = 0.15$ m, $S = 0.1$ m, $\theta = 0°$, $\epsilon = 0.4, m_p = 1, f_p = 2$.

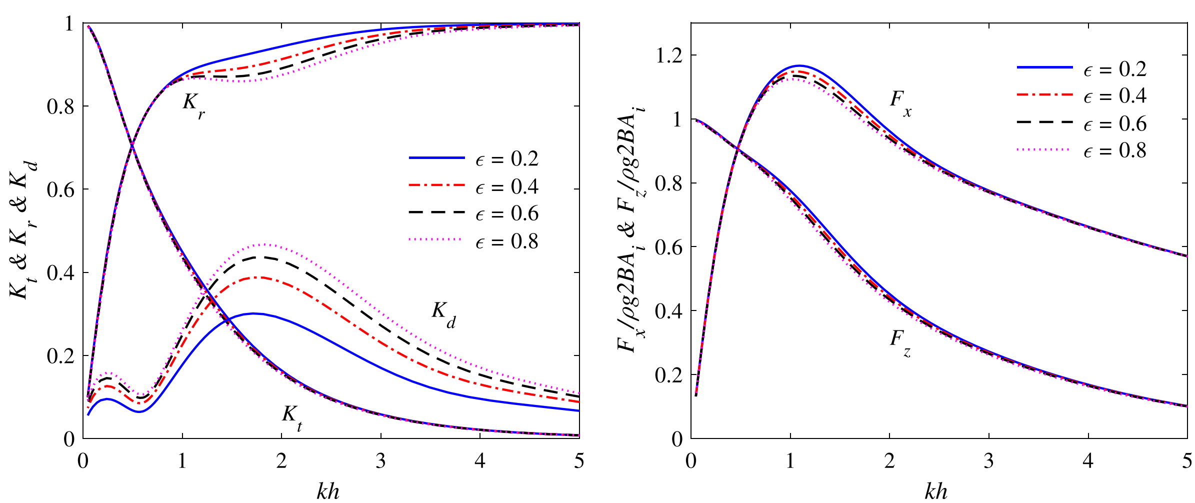

(a) Wave transmission, reflection and energy dissipation coefficient K_t, K_r and K_d (b) Horizontal and vertical wave force F_x and F_z

Fig. 18. Effects of the rubble mound foundation's porosity ϵ on K_t, K_r, K_d, F_x and F_z (through the EEBEM). $h_1 = 0.5$ m, $B/h_1 = 0.3$, $d_n/h_1 = 0.5$, $S/h_1 = 0.2$, $\theta = 0°$, $L_p/h_1 = 0.8$, $h_2/h_1 = 0.7$, $m_p = 1$, $f_p = 2$.

and θ gradually deviates from 0, J_Q first increases and then decreases and J_K decreases first and then increases. This is because, on the one hand, when the culvert is near the water surface, the wave energy near the culvert can be enhanced. On the other hand, with the decrease of culvert height, the energy of transmitted wave can also decrease. From the above, when the culvert inclined angle θ is positive (the culvert inlet is close to the water surface and the outlet is close to the water bottom), the hydrodynamics performance of the inclined culvert is better than the horizontal culvert. However, when θ is negative, the effect of culvert is weaker than that of horizontal culvert because of the weakening of water exchange.

Fig. 22 demonstrates the variations of the wave transmission evaluation value J_K, water exchange evaluation value J_Q and comprehensive evaluation value J with the change of the culvert inlet height $\Delta S/h$, for different culvert length B/h. It is found that the comprehensive evaluation value J first increases and then decreases with the increase of ΔS. The peak value of J decreases and the value of $\Delta S/h$ that matches the peak value of J increases with the increase of B/h, indicating that increasing the culvert length B is not conducive to optimize the culvert. Besides, the culvert inlet height $\Delta S/h$ has a great impact on J. When B/h = 0.3 to 0.75, $\Delta S/h$ = 0.18 to 0.25 is the best setting for the culvert.

It can be seen from the above that, in practical engineering, when the culvert inlet (sea area) is higher than the culvert outlet (harbor area), the high turbidity water at the bottom of the harbor will flow into the sea through oscillatory flow, and the low turbidity water at the surface of sea will flush the harbor area. It could be expected that due to this special setting, the VWBIC can further enhance the water exchange capacity of the harbor. Furthermore, increasing the culvert inclined angle θ can effectively reduce the wave force and make the structure safer. All these represent that the vertical wall breakwater with inclined culvert (VWBIC) is good for engineering application.

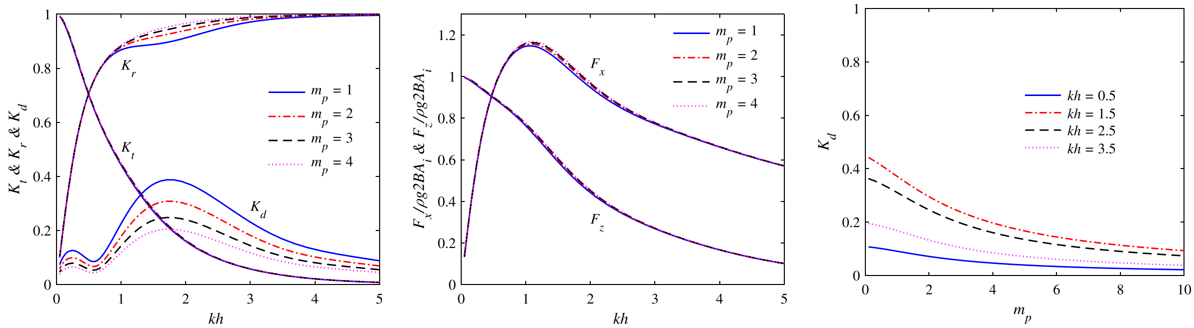

(a) Wave transmission, reflection and energy dissipation coefficient K_t, K_r and K_d

(b) Horizontal and vertical wave force F_x and F_z

(c) Wave energy dissipation coefficient K_d

Fig. 19. Effects of the rubble mound foundation's inertial coefficient m_p on K_t, K_r, K_d, F_x and F_z (through the EEBEM). $h_1 = 0.5$ m, $B/h_1 = 0.3$, $d_n/h_1 = 0.5$, $S/h_1 = 0.2$, $\theta = 0°$, $L_p/h_1 = 0.8$, $h_2/h_1 = 0.7$, $\varepsilon = 0.4$, $f_p = 2$.

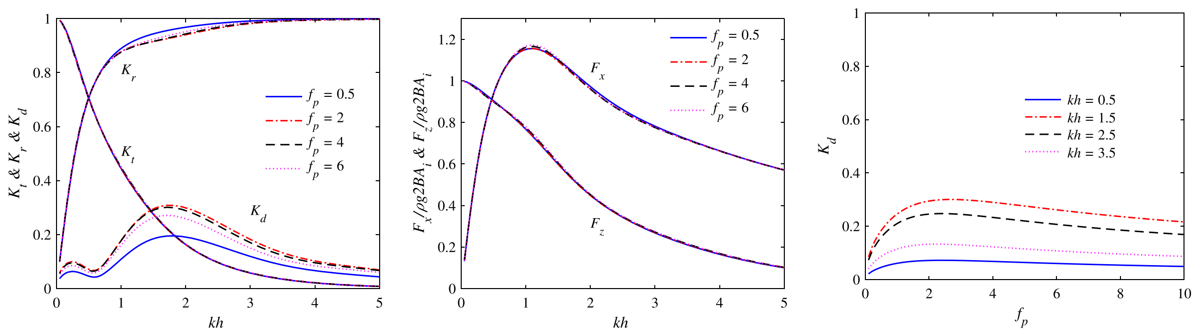

(a) Wave transmission, reflection and energy dissipation coefficient K_t, K_r and K_d

(b) Horizontal and vertical wave force F_x and F_z

(c) Wave energy dissipation coefficient K_d

Fig. 20. Effects of the rubble mound foundation's friction coefficient f_p on K_t, K_r, K_d, F_x and F_z (through the EEBEM). $h_1 = 0.5$ m, $B/h_1 = 0.3$, $d_n/h_1 = 0.5$, $S/h_1 = 0.2$, $\theta = 0°$, $L_p/h_1 = 0.8$, $h_2/h_1 = 0.7$, $\varepsilon = 0.4$, $m_p = 1$.

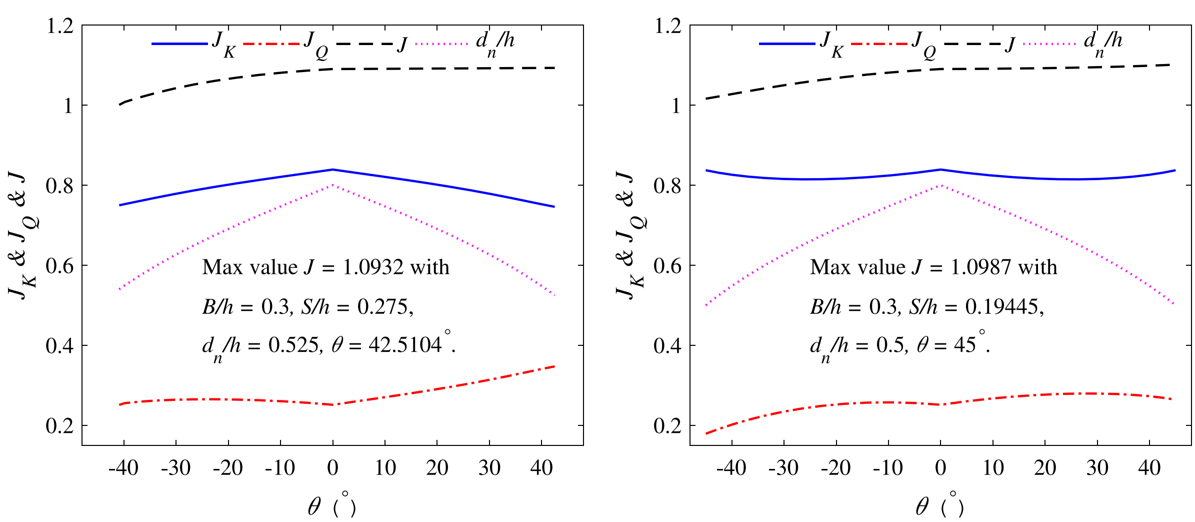

(a) Culvert height $S/h = 0.275$

(b) Culvert entrance height $\Delta S/h = 0.275$

Fig. 21. Variations of the wave transmission evaluation value J_K, water exchange evaluation value J_Q and comprehensive evaluation value J with the culvert inclined angle θ (through the EEBEM), $h_1 = h_2 = h = 0.4$ m, $B/h_1 = 0.3$, $L_p/h_1 = 0$.

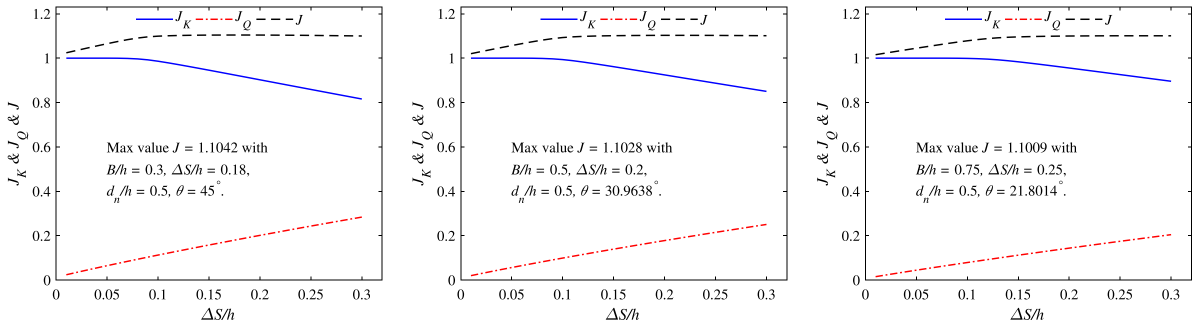

(a) $B/h = 0.3$ (b) $B/h = 0.5$ (c) $B/h = 0.75$

Fig. 22. Variations of the wave transmission evaluation value J_K, water exchange evaluation value J_Q and comprehensive evaluation value J with the culvert entrance height $\Delta S/h$, for different culvert length B/h (through the EEBEM). $h_1 = h_2 = h = 0.4$ m, $d_n/h = 0.5$, $(d_3 + d_4)/2/h = 0.8$, $L_p/h_1 = 0$.

5. Conclusions

A new-type environmentally friendly breakwater named vertical wall breakwater with inclined culvert (VWBIC) is proposed in this paper. A coupled eigenfunction expansion boundary element method (EEBEM) combining computational fluid dynamics (CFD) numerical simulations is developed to study the hydrodynamic performance of the VWBIC on a permeable rubble mound foundation. Results show that compared with vertical wall breakwater with horizontal culvert, the VWBIC can optimize the hydrodynamic performance better, which has great engineering significance. From this study, the following conclusions can be drawn:

1. When the culvert inclined angle θ is opposite, such as θ and $-\theta$, both the amplitude of the transmission wave and reflection wave are the same. But the oscillatory flow with positive inclined angle ($+\theta$) is obviously larger than that with negative inclined angle ($-\theta$), and with the increase of θ and relative water depth kh, this difference is more obvious.

2. When the culvert inclined angle θ is positive and the culvert inlet heights $\Delta S/h$ is constant, with an increase in θ, VWBIC can effectively reduce K_t of medium and long waves and promote Q_m of short waves. Besides, the peak value of F_x sharply decreases and the maximum value of F_z is almost unchanged.

3. Permeable rubble mound foundation can effectively dissipate the wave energy, reduce the reflection coefficient and wave force on the VWBIC, and maintain the stability of the structure. Especially, when the rubble mound foundation's length $L_p = L_2/4 + L_2/2 * n$ ($n = 0, 1, 2...$), the corresponding wave reflection coefficient can be significantly reduced and the energy dissipation coefficient can be obviously increased due to the resonance.

4. Culvert structural parameters corresponding to the optimal solution change with the change of the culvert inclined angle θ. Small culvert length B/h and big θ are beneficial to practical applications. Besides, the culvert inlet height $\Delta S/h$ has a great impact on the optimal solution of the culvert. When $B/h = 0.3$ to 0.75, $\Delta S/h = 0.18$ to 0.25 is the best setting for the culvert.

5. Compared with vertical wall breakwater with horizontal culvert, the VWBIC is more favorable for engineering application. It can effectively improve the stability of berthing and structure, further promote water exchange and improve the port environment.

CRediT authorship contribution statement

Chaofan Lv: Conceptualization, Methodology, Formal analysis, Investigation, Data curation, Writing – original draft, Writing – review & editing, Visualization, Project administration, Funding acquisition. **Xizeng Zhao:** Formal analysis, Writing – review & editing, Visualization, Supervision, Funding acquisition. **Mingchang Li:** Formal analysis, Writing – review & editing, Visualization, Supervision.

Declaration of competing interest

The authors declare that they have no known competing financial interests or personal relationships that could have appeared to influence the work reported in this paper.

Acknowledgments

This study was partially supported by the National Natural Science Foundation of China (Grant Nos. 51979245, 51679212) and HPC Center OF ZJU (ZHOUSHAN CAMPUS).

References

Bakhti, Y., Chioukh, N., Hamoudi, B., Boukhari, M., 2017. A multi-domain boundary element method to analyze the reflection and transmission of oblique waves from double porous thin walls. J. Mar. Sci. Appl. 16 (3), 276–285.

Bartolić, I., Lončar, G., Bujak, D., Carević, D., 2018. The flow generator relations for water renewal through the flushing culverts in marinas. Water 10 (7), 936.

Belibassakis, K.A., Tsoukala, V.K., Katsardi, V., 2014. Three-dimensional wave diffraction in the vicinity of openings in coastal structures. Appl. Ocean Res. 45, 40–54.

Carevic, D., Mostecak, H., Bujak, D., Lončar, G., 2018. Influence of water-level variations on wave transmission through flushing culverts positioned in a breakwater body. J. Waterw. Port Coast. Ocean Eng. 144 (5), 04018012.

Chen, J.-T., Yueh, C.-Y., Chang, Y.-L., Wen, C.-C., 2017. Why dual boundary element method is necessary? Eng. Anal. Bound. Elem. 76, 59–68.

Dalrymple, R.A., Losada, M.A., Martin, P., 1991. Reflection and transmission from porous structures under oblique wave attack. J. Fluid Mech. 224, 625–644.

Del Jesus, M., Lara, J.L., Losada, I.J., 2012. Three-dimensional interaction of waves and porous coastal structures: Part I: Numerical model formulation. Coast. Eng. 64, 57–72.

Deng, Z., Wang, L., Zhao, X., Huang, Z., 2019. Hydrodynamic performance of a T-shaped floating breakwater. Appl. Ocean Res. 82, 325–336.

Goda, Y., Suzuki, Y., 1976. Estimation of incident and reflected waves in random wave experiments. Plos One 4 (9), 73.

Jacobsen, N.G., Fuhrman, D.R., Fredsøe, J., 2012. A wave generation toolbox for the open-source CFD library: OpenFoam®. Internat. J. Numer. Methods Fluids 70 (9), 1073–1088.

Kashiwagi, M., Hayashi, T., 2008. Experimental confirmation of reciprocity relations of waves around an asymmetric floating body. In: 23rd Intl Workshop on Water Waves and Floating Bodies, Jeju (Korea). Citeseer, pp. 1–4.

Koley, S., Behera, H., Sahoo, T., 2015a. Oblique wave trapping by porous structures near a wall. J. Eng. Mech. 141 (3), 04014122.

Koley, S., Panduranga, K., Almashan, N., Neelamani, S., Al-Ragum, A., 2020. Numerical and experimental modeling of water wave interaction with rubble mound offshore porous breakwaters. Ocean Eng. 218, 108218.

Koley, S., Sahoo, T., 2017. Wave interaction with a submerged semicircular porous breakwater placed on a porous seabed. Eng. Anal. Bound. Elem. 80, 18–37.

Koley, S., Sarkar, A., Sahoo, T., 2015b. Interaction of gravity waves with bottom-standing submerged structures having perforated outer-layer placed on a sloping bed. Appl. Ocean Res. 52, 245–260.

Li, A.-j., Liu, Y., Li, H.-j., Fang, H., 2020. Analysis of water wave interaction with a submerged fluid-filled semi-circular membrane breakwater. Ocean Eng. 197, 106901.

Li, C., Shi, H., Wang, A., Yu, D., 1997a. Calculation of the perforated wave height for vertical perforated-pipe breakwater. J. Ocean Univ. China 27 (004), 571–577.

Li, C., Shi, H., Yu, D., Wang, A., 1997b. Calculation of wave pressure and pressure spectrum for perforate-pipe breakwater. China Ocean Eng. 11 (001), 79–88.

Liu, Y., Li, H.J., 2013. Analysis of oblique wave interaction with a submerged perforated semicircular breakwater. J. Eng. Math. 83 (1), 23–36.

Liu, P.L.-F., Lin, P., Chang, K.-A., Sakakiyama, T., 1999. Numerical modeling of wave interaction with porous structures. J. Waterw. Port Coast. Ocean Eng. 125 (6), 322–330.

Lv, C., Zhao, X., 2021. Environmentally friendly vertical wall breakwater with culvert for encircled harbor basin. J. Eng. Mech. 147 (12), 04021104.

Madsen, O.S., 1974. Wave transmission through porous structures. J. Waterw. Harbors Coast. Eng. Div. 100 (3), 169–188.

Pérez-Romero, D.M., Ortega-Sánchez, M., Moñino, A., Losada, M.A., 2009. Characteristic friction coefficient and scale effects in oscillatory porous flow. Coast. Eng. 56 (9), 931–939.

Rageh, O., Koraim, A., 2010. Hydraulic performance of vertical walls with horizontal slots used as breakwater. Coast. Eng. 57 (8), 745–756.

Requejo, S., Vidal, C., Losada, I., 2002. Modelling of wave loads and hydraulic performance of vertical permeable structures. Coast. Eng. 46 (4), 249–276.

Rodríguez, A.M., Casarín, R.S., Ilzarbe, J.B., 2022. The influence of oblique waves on the hydrodynamic efficiency of an onshore OWC wave energy converter. Renew. Energy 183, 687–707.

Sollitt, C.K., Cross, R.H., 1973. Wave transmission through permeable breakwaters. In: Coastal Engineering 1972. pp. 1827–1846.

Suh, K.D., Jung, H.Y., Chong, K.P., 2007. Wave reflection and transmission by curtainwall?pile breakwaters using circular piles. Ocean Eng. 34 (14–15), 2100–2106.

Suh, K.-D., Shin, S., Cox, D.T., 2006. Hydrodynamic characteristics of pile-supported vertical wall breakwaters. J. Waterw. Port Coast. Ocean Eng. 132 (2), 83–96.

Tsoukala, V.K., Gaitanis, C., Stamou, A.I., Moutzouris, C.I., 2010. Wave and dissolved oxygen transmission analysis in harbors using flushing culverts: An experimental approach. Global Nest J. 12 (2), 152–160.

Tsoukala, V.K., Katsardi, V., Belibassakis, K.A., 2014. Wave transformation through flushing culverts operating at seawater level in coastal structures. Ocean Eng. 89 (oct.1), 211–229.

Tsoukala, V.K., Moutzouris, C.I., 2008. A 3-D experimental study on the beneficial role of flushing culverts in sea water quality. In: 31st International Conference on Coastal Engineering, ICCE 2008.

Tsoukala, V.K., Moutzouris, C.I., 2009. Wave transmission in harbors through flushing culverts. Ocean Eng. 36 (6–7), 434–445.

Xie, B., Ii, S., Ikebata, A., Xiao, F., 2014. A multi-moment finite volume method for incompressible Navier–Stokes equations on unstructured grids: volume-average/point-value formulation. J. Comput. Phys. 277, 138–162.

Zhang, Z., Zhao, X., Xie, B., Nie, L., 2019. High-fidelity simulation of regular waves based on multi-moment finite volume formulation and THINC method. Appl. Ocean Res. 87, 81–94.

Zhao, Y., Liu, Y., Li, H., 2016. Wave interaction with a partially reflecting vertical wall protected by a submerged porous bar. J. Ocean Univ. China 15 (4), 619–626.

Zhao, Y., Liu, Y., Li, H.-J., Chang, A.-T., 2020. Iterative dual BEM solution for water wave scattering by breakwaters having perforated thin plates. Eng. Anal. Bound. Elem. 120, 95–106.

Zhao, X., Ye, Z., Fu, Y., Cao, F., 2014. A CIP-based numerical simulation of freak wave impact on a floating body. Ocean Eng. 87, 50–63.

Zhu, S., Chwang, A.T., 2001. Investigations on the reflection behaviour of a slotted seawall. Coast. Eng. 43 (2), 93–104.